AUTOPHAGY
2019, VOL. 15, NO. 6, 1031–1050
https://doi.org/10.1080/15548627.2019.1569929

Taylor & Francis
Taylor & Francis Group

RESEARCH PAPER

Gyp1 has a dual function as Ypt1 GAP and interaction partner of Atg8 in selective autophagy

Anne Lisa Mitter, Petra Schlotterhose, and Roswitha Krick

Department of Cellular Biochemistry, University Medicine, Georg-August University, Goettingen, Germany

ABSTRACT

Macroautophagy/autophagy is a highly conserved intracellular vesicle transport pathway that prevents accumulation of harmful materials within cells. The dynamic assembly and disassembly of the different autophagic protein complexes at the so-called phagophore assembly site (PAS) is strictly regulated. Rab GTPases are major regulators of cellular vesicle trafficking, and the Rab GTPase Ypt1 and its GEF TRAPPIII have been implicated in autophagy. We show that Gyp1 acts as a Ypt1 GTPase-activating protein (GAP) for selective autophagic variants, such as the Cvt pathway or the selective autophagic degradation of mitochondria (mitophagy). Gyp1 regulates the dynamic disassembly of the conserved Ypt1-Atg1 complex. Thereby, Gyp1 sets the stage for efficient Atg14 recruitment, and facilitates the critical step from nucleation to elongation of the phagophore. In addition, we identified Gyp1 as a new Atg8-interacting motif (AIM)-dependent Atg8 interaction partner. The Gyp1 AIM is required for efficient formation of the cargo receptor-Atg8 complexes. Our findings elucidate the molecular mechanisms of complex disassembly during phagophore formation and suggest potential dual functions of GAPs in cellular vesicle trafficking.

Abbreviations AIM, Atg8-interacting motif; Atg, autophagy related; Cvt, cytoplasm-to-vacuole targeting; GAP, GTPase-activating protein; GEF, guanine-nucleotide exchange factor; GFP, green fluorescent protein; log phase, logarithmic growth phase; NHD, N-terminal helical domain; PAS, phagophore assembly site; PE, phosphatidylethanolamine; PtdIns3P, phosphatidylinositol-3-phosphate; WT, wild-type

ARTICLE HISTORY
Received 12 February 2018
Revised 1 November 2018
Accepted 7 January 2019

KEYWORDS
Atg1; autophagy; cargo receptor; Rab GTPase; yeast; Ypt1

Introduction

Macroautophagy (hereafter autophagy) is essential for removal of harmful materials, such as protein aggregates, damaged mitochondria, or invasive bacteria within cells. Therefore, autophagy defects are linked to various human disease [1–5]. The cargo is selectively or non-selectively enwrapped by a unique double-membrane compartment, the phagophore. This structure matures into an autophagosome, which transports the cargo to the lysosome for its degradation. Genetic screens for autophagy-defective mutants in yeast and other fungi have at present identified more than 40 autophagy-related (*ATG*) genes that comprise the core machinery and specific components for the selective variants of autophagy. Autophagosome formation is initiated at the so-called phagophore assembly site (PAS), where the Atg proteins localize at least transiently [6,7].

The best-characterized type of selective autophagy is the cytoplasm-to-vacuole targeting (Cvt) pathway that serves as a prototype for selective autophagy in yeast [8]. The Cvt pathway acts under nutrient-rich conditions and delivers specific enzymes, such as the precursor form of aminopeptidase I (prApe1), to the vacuole, where they are matured to execute their enzymatic functions. The dynamic assembly and disassembly of the Atg protein complexes requires various protein-protein interactions that are strictly organized. prApe1 is bound by its cargo receptor Atg19 in the cytosol to form the so-called Cvt complex [9–12]. Atg11, a coiled-coil tethering protein, interacts with Atg19 and at least 5 additional Atg proteins to organize Cvt vesicle biogenesis [13,14]. One of the Atg11 interactors is the serine/threonine kinase Atg1 that is critical for phagophore initiation [15,16]. Atg11 further interacts with the Rab GTPase Ypt1 [17–20]. Ypt1 in return also interacts with Atg1 [21]. Rab GTPases such as Ypt1 act as molecular switches in membrane trafficking. Only active GTP-bound Ypt1 efficiently interacts with its effectors Atg11 and Atg1 [18,21]. Rab GTPases such as Ypt1 are activated by guanine-nucleotide exchange factors (GEFs). The Trs85-containing transport protein particle III (TRAPPIII) complex has been determined to be an autophagy-specific GEF for Ypt1 [19,22–25], although recently an additional TRAPP subunit, Trs33, has been implicated in autophagy [22,26–28]. Furthermore, a role of TRAPPIII in Ypt1 activation during ER-Golgi transport has been proposed [29]. Rab GTPases are inactivated by GTPase-activating proteins (GAPs) [30–32]. The GAPs Gyp1, Gyp5, and Gyp8 stimulate the hydrolysis of GTP on Ypt1 [33–35]. Gyp1 has been proposed to regulate Ypt1 at the Golgi [34], and has been recently implicated in autophagy-related pathways [36]. When Ypt1 is inactivated during autophagic processes is unclear.

CONTACT Roswitha Krick roswitha.krick@med.uni-goettingen.de Department of Cellular Biochemistry, University Medicine, Georg-August University, Goettingen, Germany

Supplemental data for this article can be accessed here.

Dependent on the Atg1 kinase complex, PAS assembly proceeds by recruitment of Atg14 and thereby the autophagy-specific class III phosphatidylinositol 3-kinase (PtdIns3K) complex [37–40]. Under nutrient-rich conditions the phosphatidylinositol-3-phosphate (PtdIns3P) signal is decoded by the yeast PROPPIN (β-propellers that bind phosphoinositides) Atg21 [41]. Atg21 recruits the ubiquitin-like protein Atg8 to the PAS and organizes its conjugation to phosphatidylethanolamine (PE) [42]. Atg8–PE has different roles in phagophore formation during selective autophagy. This protein is, for example, required to tether receptor-bound cargo complexes to the concave side of the phagophore and for phagophore expansion [43–49]. Atg8–PE is also part of the coat-like structure at the convex side of the phagophore [50]. Atg8-interacting motifs (AIMs), composed of a WxxL-like motif, have been identified in most of the Atg8-interacting proteins. Atg8 in turn contains 2 hydrophobic pockets in its C-terminal ubiquitin-like domain that form the AIM-binding site [51–55]. A conserved FK-motif in the N-terminal helical domain (NHD) of Atg8 is also required for some protein interactions [42,56]. How the different Atg8 interactions are organized and how Atg8–PE is directed from the lipidation complex to its different functional sites is still unclear.

In this study, we show that the GAP activity of Gyp1 is required for selective autophagy. Gyp1 regulates the dynamic disassembly of the conserved Ypt1-Atg1 complex as a prerequisite for proper Atg14 recruitment to the PAS. In addition, we identified Gyp1 as new AIM-dependent Atg8 interaction partner and mapped the AIM in Gyp1. Mutation of the Gyp1 AIM precluded efficient formation of cargo receptor-Atg8–PE complexes. We propose that the Gyp1-Atg8 interaction is involved in directing Atg8–PE from the lipidation complex to the cargo receptor complexes.

Results

How is the presence of Atg8 in different complexes regulated? We postulated the presence of a regulatory protein. Therefore, we precipitated potential Atg8 interaction partners out of crude extracts from wild-type (WT) yeast cells using recombinant GST-tagged Atg8 or GST alone as a control and tested for interacting proteins. Mass spectrometry analysis revealed the GAP Gyp1 in the elution fraction of 2 independent samples. We followed this hint as the GAP Gyp1 stimulates the hydrolysis of GTP on the Rab GTPase Ypt1, a regulator of vesicle trafficking involved in autophagy [33–35].

Gyp1 and Atg8 interact via L50 of Atg8

The interaction of Atg8 and Gyp1 was first verified *in vivo*. We included 2 other potential Ypt1 GAPs, Gyp5 and Gyp8 [33], in the analysis to determine the specificity of the Gyp1-Atg8 interaction. Gyp1-HA, Gyp5-HA and Gyp8-HA were co-immunoprecipitated with GFP-Atg8 or GFP alone out of cells grown to logarithmic (log) phase. None of the GAPs precipitated with GFP alone. Gyp5-HA showed no binding and Gyp8-HA bound only very weakly to GFP-Atg8. Instead, Gyp1-HA clearly bound to immobilized GFP-Atg8 (Figure 1(a,b)). These results show a preferential interaction of Atg8 with Gyp1 *in vivo*.

We confirmed that Atg8 preferentially interacts with Gyp1 *in vitro*. Therefore, yeast crude extracts from cells containing HA-tagged Gyp1, Gyp5 or Gyp8 were incubated with immobilized GST-Atg8 and GST alone as a negative control. Again, none of the GAPs bound to GST. Gyp5-HA and Gyp8-HA showed only weak binding to GST-Atg8, but Gyp1-HA efficiently bound to GST-Atg8 (Figure S1A-B). Taken together, we identify Gyp1 as novel Atg8 interaction partner.

Next, we determined the binding site for Gyp1 in Atg8 *in vivo*. Again, GFP alone did not precipitate Gyp1-HA. Gyp1-HA showed WT-like binding to the NHD control mutant, GFP-Atg8^{S3,T4A}, with mutations in non-conserved amino acids. A reduced amount of Gyp1-HA co-precipitated with GFP-Atg8^{F5,K6G} (43%), carrying mutations in conserved amino acids of the Atg8 NHD. GFP-Atg8^{L50A} and GFP-Atg 8^{Y49A}, both mutated in the AIM-binding site, co-precipitated significantly less Gyp1-HA (9% and 5%) compared to GFP-Atg8 (Figure 1(c,d)). This result indicates, that the interaction with Gyp1 mainly requires the AIM-binding site of Atg8, and in addition the Atg8 NHD.

We further confirmed the L50-dependent Gyp1-Atg8 interaction under endogenous conditions. Therefore, the *GFP-ATG8* variants and *GFP* alone were expressed from the *ATG8* promoter, and the quantity of cells was increased to saturate the beads. Binding of Gyp1-HA to GFP-Atg8^{L50A} and to GFP alone was significantly reduced to 37% and 33% compared to GFP-Atg8 (Figure 1(e,f)). This result also stresses the reliability of the experiments with overexpressed Atg8. Taken together, we demonstrate a novel interaction between Atg8 and Gyp1.

Mapping of AIM1 in Gyp1, required for direct interaction with Atg8

In order to detect the residues in Gyp1 important for the interaction with Atg8, we used the *iLIR* web server [57], that predicted potential AIMs in Gyp1. The first and the last amino acid of the WxxL motif from 7 highly conserved potential AIMs in Gyp1 were exchanged with alanine (Figure S2A, C). We noted that mutation of AIM2 and AIM4 to AIM7 destabilized the protein, and thus are not reliable for analysis (Figure 2(a), Figure S2B). Conversely, Gyp1[AIM1]-HA and Gyp1[AIM3]-HA were stable and we tested their binding to GFP-Atg8; we included one destabilized mutant, Gyp1[AIM2]-HA. In some of the replicates, mutation of Gyp1 AIM3 increased binding to GFP-Atg8 (178%) compared to the Gyp1 WT. Interestingly, mutation of Gyp1 AIM1 abolished binding to GFP-Atg8 (4%; Figure 2(a,b)). Thus, we conclude that AIM1, highly conserved among yeasts (Figure 2(c)), serves as an interaction site for Atg8 *in vivo*.

To test the results for AIM1 and AIM3 using a different approach, we analyzed binding of Gyp1[AIM1] and Gyp1 [AIM3] to Atg8 *in vitro* and again included one destabilized mutant, Gyp1[AIM2]. Immobilized GST-Atg8 and GST alone were incubated with the indicated yeast crude extracts. Again, no binding of the Gyp1 WT to GST alone was detected. Using this approach Gyp1[AIM3]-HA bound like the Gyp1 WT to

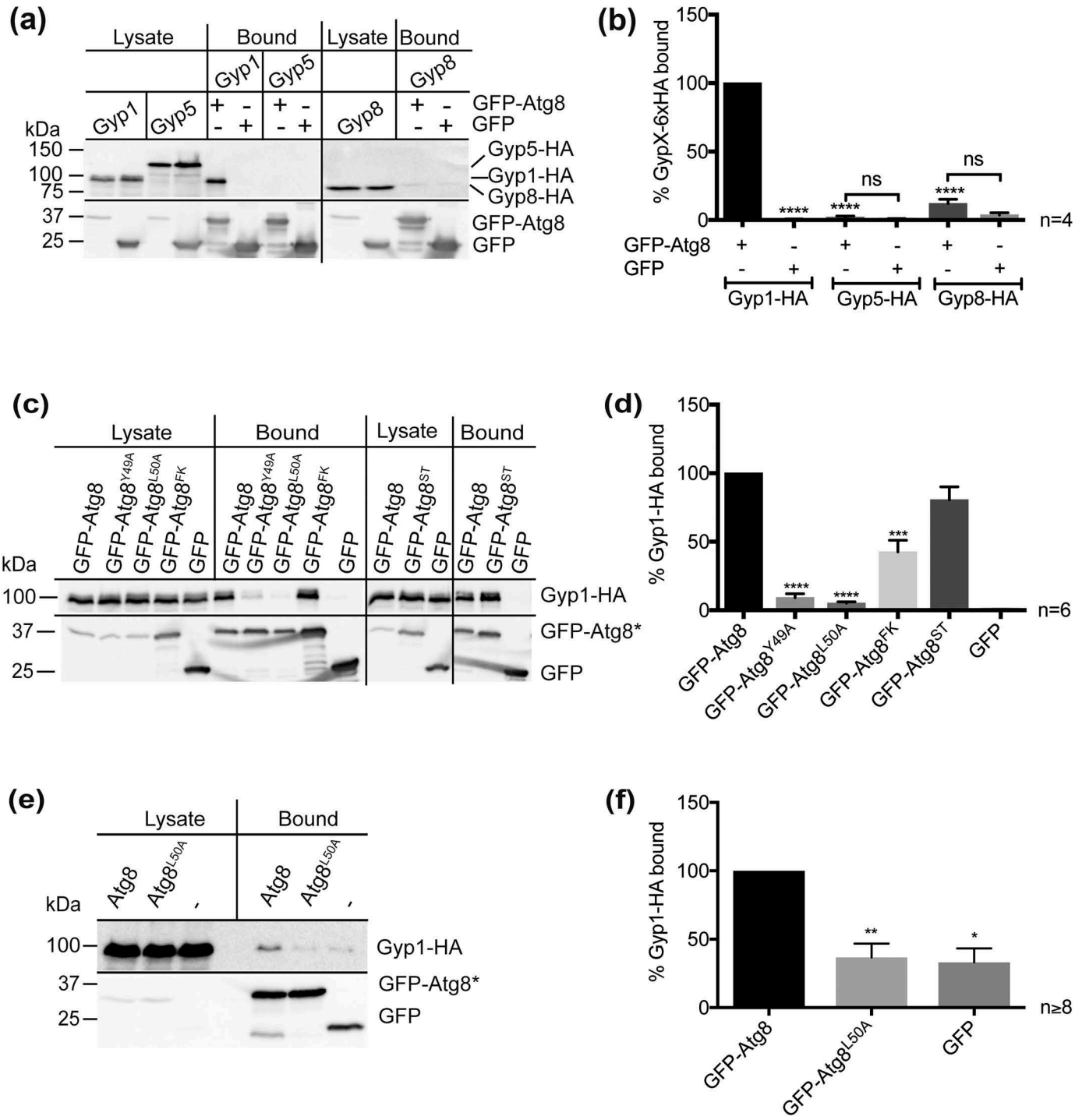

Figure 1. Gyp1 and GFP-Atg8 interact via Atg8 L50. (a) *GFP-ATG8* or *GFP* alone were expressed in cells containing *GYP1*, *GYP5* or *GYP8* chromosomally tagged with *HA*. The proteins were precipitated out of cells grown to logarithmic (log) phase with a GFP-binding protein on beads (GFP beads). (b) Quantification of (a). The amount of Gyp1-HA bound to GFP-Atg8 was set to 100%. (c) GFP-Atg8 variants or GFP alone and Gyp1-HA were co-immunoprecipitated with GFP beads out of *atg8*Δ cells grown to log phase. (d) Quantification of (c). The amount of Gyp1-HA bound to GFP-Atg8 was set to 100%. (e) *GFP-ATG8*, *GFP-ATG8*^{L50A} and *GFP* alone were expressed from the *ATG8* promoter in the *GYP1-HA* background. Proteins were co-immunoprecipitated with GFP beads out of cells grown to log phase. (f) Quantification of (e). The amount of Gyp1-HA bound to GFP-Atg8 was set to 100%. Immunoblots were probed with HA (top) or GFP antibodies (bottom). Molecular mass markers are in kDa. Asterisks or X indicate different protein variants. FK, F5G K6G; ST, S3A T4A.

GST-Atg8. Binding of Gyp1[AIM1]-HA to GST-Atg8 was significantly reduced (63%; Figure 2(d,e)). Taken together, we conclude that Gyp1 AIM1 acts as a functional AIM.

We now also tested if the Gyp1 GAP activity influences Atg8 binding by mutating R343, that is essential for its GAP activity [34]. Gyp1^{R343K}-HA bound like the Gyp1 WT to GST-Atg8 (Figure 2(f,g)). In addition, Gyp1^{R343K}-HA bound like the Gyp1 WT to GFP-Atg8 on beads, co-precipitated out of growing cells (Figure S3A-B). This indicates, that the GAP activity of Gyp1 does not influence Atg8 binding *in vitro* and *in vivo*.

Next, we used *E. coli*-expressed Gyp1 and Atg8 to show their direct interaction. Immobilized His-Gyp1, His-Gyp1

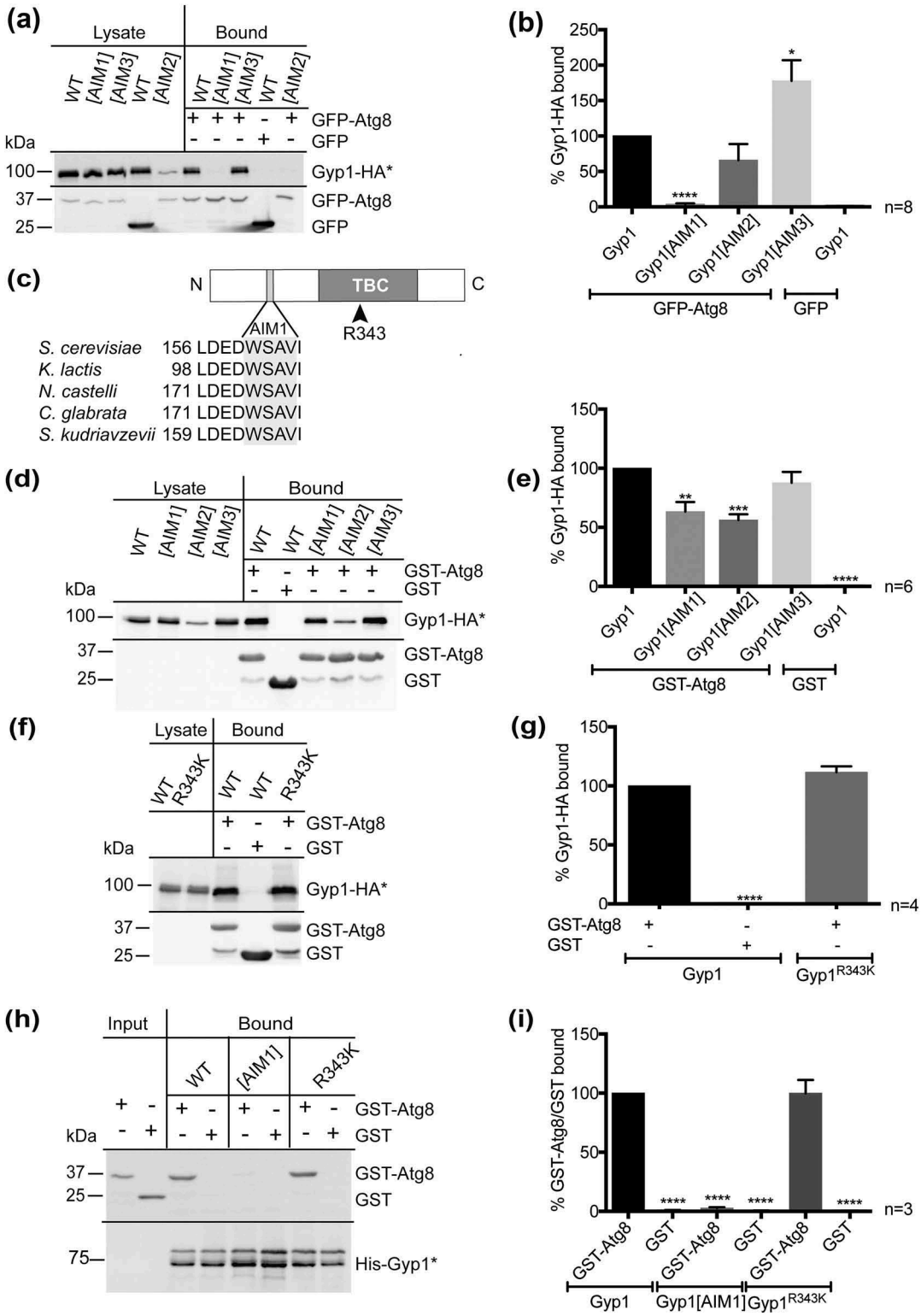

Figure 2. Mapping of AIM1 in Gyp1, required for direct interaction with Atg8. (a) *GYP1-HA* and the indicated AIM-mutants under control of the *GYP1* promoter and *GFP-Atg8* or *GFP* alone were expressed in *gyp1*Δ *atg8*Δ cells grown to log phase. Proteins were co-immunoprecipitated with GFP beads. (b) Quantification of (a). The amount of Gyp1-HA bound to GFP-Atg8 was set to 100%. (c) Schematic drawing of *S. cerevisiae* Gyp1 and sequence alignment of the Gyp1 AIM1 motif (light gray box) from various yeasts. The position of the characteristic TBC (Tre2-Bub2-Cdc16) domain, is shown (277–510). Residue R343, essential for the GAP activity of Gyp1, is marked by an arrow. (d) Immobilized GST-Atg8 or GST alone were incubated with yeast crude extract from cells grown to log phase expressing HA-tagged Gyp1 or Gyp1[AIM1], Gyp1[AIM2] or Gyp1[AIM3] from the endogenous promoter. (e) Quantification of (d). The amount of Gyp1 bound to GST-Atg8 was set to 100%. (f) Immobilized GST-Atg8 and GST alone isolated out of *E. coli* were incubated with yeast crude extract from cells grown to log phase expressing HA-tagged Gyp1 or Gyp1^{R343K} from the endogenous promoter. (g) Quantification of (f). The amount of Gyp1 bound to GST-Atg8 was set to 100%. (h) Immobilized His-tagged Gyp1 WT, Gyp1[AIM1] or Gyp1^{R343K} and soluble GST-tagged Atg8 or GST isolated out of *E. coli* were incubated. (i) Quantification of (h). The amount of GST-Atg8 bound to His-Gyp1 was set to 100%. Molecular mass markers are in kDa. Immunoblots were probed with HA, His or GST antibodies. Asterisks indicate different protein variants.

[AIM1] and His-Gyp1^{R343K} were incubated with soluble GST-Atg8 or GST alone. GST-Atg8 bound comparably to Gyp1 and Gyp1^{R343K} but not to GST alone. GST-Atg8 showed strongly reduced binding to Gyp1[AIM1] (3%), confirming that AIM1 is required for direct interaction of Gyp1 and Atg8 (Figure 2(h,i)).

We furthermore confirmed, that Gyp1[AIM1] is still able to directly interact with Ypt1. Immobilized His-Gyp1, His-Gyp1[AIM1] and His-Gyp1^{R343K} were incubated with GST-Ypt1 in its GDP- or GTP-bound form, and with GST alone. Gyp1^{R343K} was used as an additional control, as R343K is a catalytically rather than a structurally important residue, allowing its proper interaction with GTP-bound Ypt1 [58]. GST-Ypt1 in its GTP-bound form showed enhanced binding to all Gyp1 variants. The enhanced interaction of Gyp1 [AIM1] with GTP-loaded Ypt1 indicates that the mutated AIM1 motif does also not interfere with the structural integrity of Gyp1 (Figure S3C).

Gyp1 GAP activity and AIM1 are required for efficient mitophagy

Next, we asked whether the Gyp1-Atg8 interaction and also the Gyp1 GAP activity are relevant for autophagy, because the mammalian TBC domain-containing protein TBC1D14 showed a GAP-independent function in autophagy [59,60]. First, we tested the deletion strain for a prApe1 maturation defect [61], and included the other 2 Ypt1 GAPs, Gyp5 and Gyp8, in the analysis to determine the specificity of Gyp1. An *atg1*Δ strain, where prApe1 maturation is blocked, was used as a negative control. Deletion of *GYP5* alone had no effect, and deletion of *GYP8* alone (95% Ape1) or *GYP5* and *GYP8* (92% Ape1) had only very slight effects on prApe1 maturation. In contrast, the lack of Gyp1 alone already significantly reduced the amount of Ape1 to 76% under logarithmic growth conditions. Additional deletion of *GYP5* or *GYP8* in *gyp1*Δ cells increased the maturation defect slightly but significantly (69% or 56% Ape1). In *gyp1*Δ *gyp5*Δ *gyp8*Δ cells the amount of Ape1 was strongly reduced to 28% (Figure 3(a,b)). Upon nitrogen starvation, none of the deletion strains showed a prApe1 maturation defect using this approach (Figure S4A-B). This experiment was done in the WCG background, but BY4741 cells showed the same phenotypes. Therefore, Gyp1 plays the major role in the Cvt pathway, whereas Gyp5 and Gyp8 may act on Ypt1 only in the absence of Gyp1.

To further confirm, that the Cvt pathway requires the conversion of Ypt1 into its GDP-bound inactive form, we compared the prApe1 maturation defect of the *gyp1*Δ *gyp5*Δ *gyp8*Δ cells to a strain carrying the *YPT1*^{Q67L} allele. This Ypt1 mutant is mostly found in the active GTP-bound state [35,62]. We used both mating types of the Ypt1^{Q67L} strain and compared them with the corresponding WT (MSUC-3D), the *gyp1*Δ *gyp5*Δ *gyp8*Δ strain and its corresponding BY4741 WT. Convincingly, Ypt1^{Q67L} caused the same effect on prApe1 maturation as the *gyp1*Δ *gyp5*Δ *gyp8*Δ strain. The prApe1 maturation rate was reduced to 30% under logarithmic growth conditions, where the Cvt pathway is active, but no effect was detectable under starvation conditions (Figure S4C-D).

Next, we expressed different *GYP1* variants from the endogenous promoter in *gyp1*Δ and *gyp1*Δ *gyp5*Δ *gyp8*Δ cells grown to log phase. Gyp1 and the Gyp1[AIM1] mutant complemented the prApe1 maturation defect. Gyp1^{R343K}, lacking the GAP activity, significantly reduced the amount of Ape1 to 67% in the *gyp1*Δ strain and to 45% in the *gyp1*Δ *gyp5*Δ *gyp8*Δ cells (Figure 3(c,d)). The experiment was done in the WCG background, but BY4741 cells yielded the same result. Taken together, we show that efficient flux of the Cvt pathway requires the Gyp1 GAP activity.

We further overexpressed *GYP1* from the constitutive *GPD1* (glyceraldehyde-3-phosphate dehydrogenase) promoter to gain dominantly inactive GDP-bound Ypt1. The amount of Ape1 was significantly reduced (49%) compared to the WT under logarithmic growth conditions. Control cells overexpressing *GYP7*, a GAP that is not involved in Ypt1 inactivation [63], showed no effect on prApe1 maturation (Figure S4E-F). Upon nitrogen starvation, only *atg1*Δ cells showed a prApe1 maturation defect in this assay (Figure S4E and G) [64]. Together, these results show the importance of an appropriate amount of Gyp1 under logarithmic growth conditions.

Furthermore, we detected no significant defect in the degradation of GFP-Atg8 in *gyp1*Δ and *gyp1*Δ *gyp5*Δ *gyp8*Δ cells, even after shorter times of starvation, although this was recently reported [36]. We included the *atg21*Δ strain as an additional control, where autophagy is only retarded under starvation conditions [64]. This mutant showed a complete block after 2 h of starvation comparable to the *atg1*Δ strain (Figure S5A-B). Starvation-induced Atg8 expression and its selective targeting to phagophores might lead to overestimation of the autophagic rate. Therefore, we also used the non-selective cargo Pgk1-GFP to follow non-selective macroautophagy [65]. The *atg21*Δ control strain showed a strong reduction to 15% after 2 h of starvation and 43% after 4 h of starvation. Again, we could only detect very mild defects after 2 and 4 h of starvation in *gyp1*Δ and *gyp1*Δ *gyp5*Δ *gyp8*Δ cells (Figure 3(e,f)).

Gyp1 has been implicated in Ypt1 function at the Golgi, and a mild Prc1/CPY transport defect and secretion phenotype have been described for *gyp1*Δ cells [29,33,34]. This defect may point to an indirect effect of the *GYP1* deletion on Cvt vesicle biogenesis [66,67]. Therefore, we analyzed the Prc1/CPY phenotype under nutrient-rich conditions. Only the *vps21*Δ control strain secreted a significant amount of Prc1/CPY. The *gyp5*Δ and *gyp8*Δ strains showed no Prc1/CPY secretion, and the *gyp1*Δ strain secreted only minimal amounts of Prc1/CPY. Importantly, this mild Prc1/CPY secretion phenotype was not increased by additional deletion of *GYP5* and *GYP8* (Figure S6A), although the prApe1 maturation defect was significantly enhanced (Figure 3(a,b)). In addition, we analyzed Prc1/CPY maturation of the corresponding strains under logarithmic growth conditions by western blot analysis. Only the *pep4*Δ strain showed a defect in the maturation of Prc1/CPY. The presence of WT-like amounts of mature Prc1/CPY in *gyp1*Δ and *gyp1*Δ *gyp5*Δ *gyp8*Δ cells (Figure S6B-C) ruled out the possibility that the prApe1 maturation defect is due to disturbed vacuolar proteolysis.

As our results argue for a role of Gyp1 as a major Ypt1 GAP in selective autophagy, we continued our analysis using

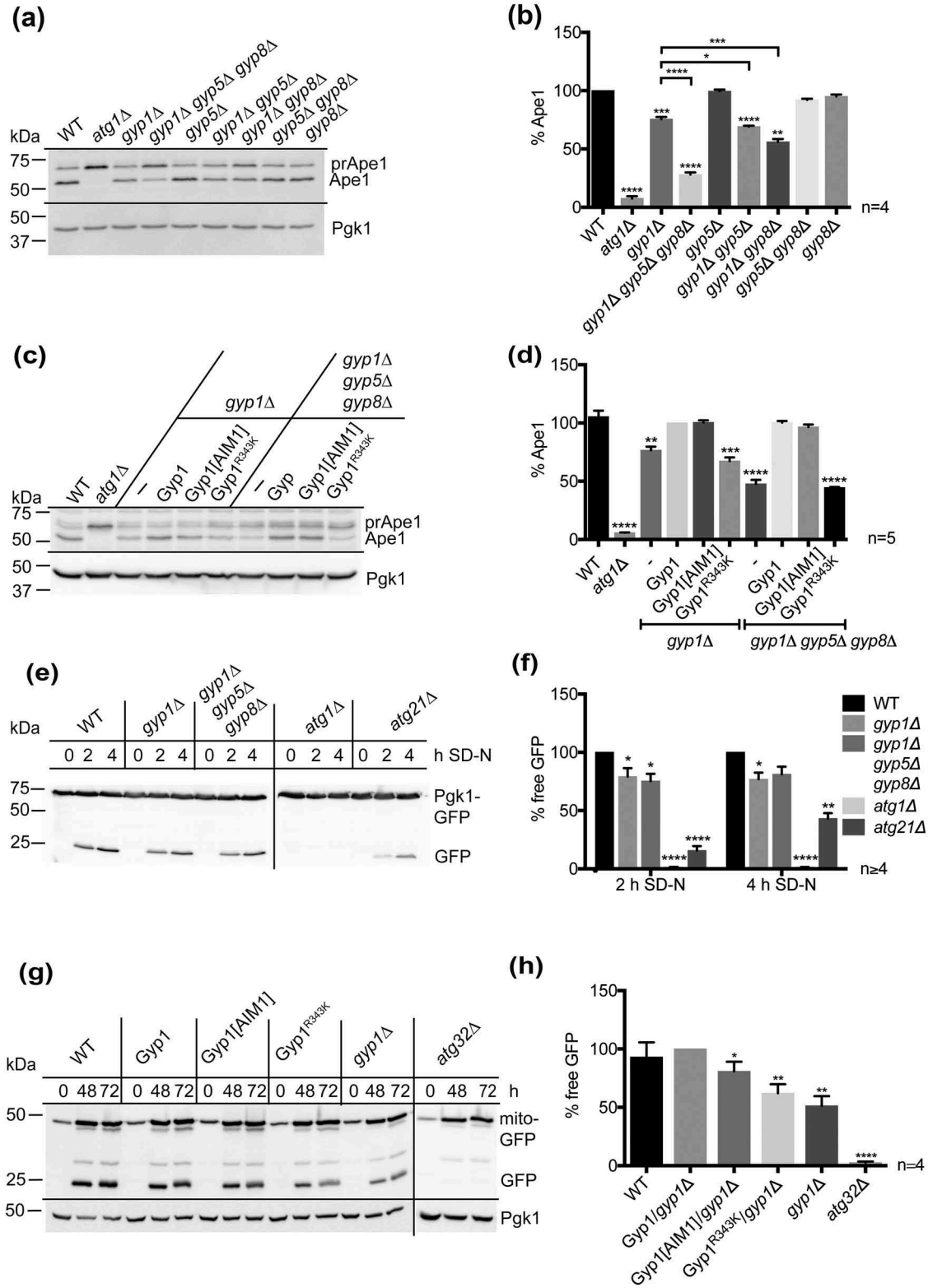

Figure 3. Gyp1 is required for efficient selective autophagy. (a) Log phase cell extracts of the indicated strains are immunoblotted with anti-Ape1 (top) and anti-Pgk1 (3-phosphoglycerate kinase; bottom). WT and *atg1*Δ cells were used as controls. (b) Quantification of (a). The percentage of Ape1 was set to 100% for the WT. (c) Gyp1, Gyp1[AIM1] and Gyp1^{R343K} under control of the *GYP1* promoter or empty vector were expressed in *gyp1*Δ and *gyp1*Δ *gyp5*Δ *gyp8*Δ cells under growing conditions and the cell extracts were immunoblotted with anti-Ape1 (top) and anti-Pgk1 (bottom). WT and *atg1*Δ cells were used as control. (d) Quantification of (c). The percentage of Ape1 was set to 100% for the WT. (e) Cell extracts of the indicated strains expressing Pgk1-GFP after 0, 2 and 4 h of starvation in SD-N were immunoblotted with anti-GFP. (f) Quantification of (e). The percentage of free GFP after 2 and 4 h of starvation was set to 100% for the WT. (g) *GYP1*-deleted cells expressing the mitophagy marker mito-GFP and either empty vector (-), Gyp1, Gyp1[AIM1] or Gyp1^{R343K} were analyzed under post-log conditions. WT and *atg32*Δ cells, depleted for the mitophagy receptor, were used as controls. Samples were taken after 0, 48 and 72 h in lactate medium. The blots were labelled with antibodies against GFP (top) and Pgk1 (bottom) as loading control. (h) Quantification of (g). The mitophagic rate as the amount of free GFP was determined after 48 h in lactate medium and set to 100% in the *gyp1*Δ strain containing Gyp1.

post-log phase-induced mitophagy and analyzed *GYP1* deleted cells containing the mitophagy marker mito-GFP and either an empty plasmid (-), or a plasmid encoding Gyp1, Gyp1[AIM1] or Gyp1^{R343K}. The mitophagic rate was determined after 48 h in lactate medium and was strongly reduced to 2.5% in *atg32*Δ cells, lacking the mitophagy receptor [68]. Deletion of *GYP1* significantly reduced the mitophagic rate to 51% (Figure 3(g,h)). Expression of *GYP1* again complemented the *gyp1*Δ phenotype. Interestingly, not only the abolished GAP activity (Gyp1^{R343K}) reduced the mitophagic rate to 62%, but also Gyp1[AIM1] caused a significant reduction to 81%. (Figure 3(g,h)). We conclude that both, the Gyp1 GAP activity and its interaction with Atg8, are required for efficient selective mitophagy.

Gyp1 colocalizes with Atg8 at the Cvt-specific PAS

Gyp1 resides on multiple punctate structures that might represent the Golgi. Additionally, GFP-Gyp1 has been localized to the PAS [34–36]. We quantitatively evaluated the colocalization of Gyp1 with 2 different PAS markers to analyze the effect of Gyp1[AIM1] and Gyp1^{R343K} using fluorescence microscopy.

First, we tested the colocalization of Gyp1 and its interaction partner Atg8, that is also considered as a PAS marker. Approximately 30% of the GFP-Atg8 dots colocalized with one of the Cherry-Gyp1 dots in cells grown to log phase. Neither mutation of Gyp1 AIM1 nor an abolished GAP activity caused a significant difference in the colocalization rate (Figure 4(a,b)). We conclude that a part of Gyp1 colocalizes with its interaction partner Atg8 at the PAS. We confirmed the localization of Gyp1 to the Cvt-specific PAS by analyzing the percentage of prApe1-RFP dots that colocalize with one of the GFP-Gyp1 dots in cells grown to log phase. A colocalization rate of approximately 50% was detected with no significant difference for GFP-Gyp1[AIM1] or Gyp1^{R343K}. Furthermore, the colocalization rate of GFP-Gyp1 and prApe1-RFP was independent of the Gyp1 interaction partner Atg8 analyzed in *gyp1*Δ *atg8*Δ cells (Figure 4(c,d)). These results emphasize a direct role of Gyp1 in selective autophagy and indicate that a pool of Gyp1 localizes to the Cvt-specific PAS, independent of the Gyp1 GAP activity or its AIM.

However, it is likely that Gyp1 is primarily recruited to the Golgi and the Cvt-specific PAS by its TBC-domain-mediated interaction with Ypt1 [69]. Thereby, an effect of Gyp1[AIM1] on the Gyp1 PAS localization might be masked. We created GFP-Gyp1[1–238], lacking the TBC domain but containing the N terminus of Gyp1 with the AIM1 motif and GFP-Gyp1 [AIM1 1–238], additionally carrying the AIM1 mutation. The constructs were even more stable than the full-length proteins (Figure S7A) and no longer showed multiple dots but instead a strong cytosolic signal and at most one single dot per cell (Figure 4(e)). We again analyzed the percentage of prApe1-RFP dots that colocalize with these residual GFP-Gyp1 dots. Interestingly, the colocalization rate decreased significantly to approximately 30% in cells containing the AIM1 mutant compared to the WT (Figure 4(f)). This decrease was in line with a significantly reduced number of GFP-Gyp1[AIM1 1–238] dots/cell (Figure 4(g)).

In contrast, we could not detect a significant difference in the number of prApe1 dots/cell (Ape1 rate) between both truncated versions, and the Ape1 rate was also independent of Gyp1[AIM1] or the Gyp1 GAP activity. Deletion of *ATG8* led to a significant increase in the Ape1 rate, in line with a block in the Cvt pathway (Figure S7B). We conclude, that a pool of Gyp1 localizes to the Cvt-specific PAS, where the interaction of Gyp1 and Atg8 occurs in living cells. Upon elimination of the Ypt1-Gyp1 interaction using the truncated Gyp1 variants we could further show an effect of the mutated Gyp1[AIM1] on the Gyp1 PAS localization. Although, our results with full-length Gyp1[AIM1] clearly suggest that the main PAS localization motif resides in the C-terminal part of Gyp1, containing the TBC domain.

The Gyp1 GAP activity is required for efficient disassembly of the Ypt1-Atg1 complex

The serine/threonine kinase Atg1, that is critical for phagophore initiation [15,16], and Atg11, the scaffold protein essential for the Cvt pathway [13,14], have been recently described as effectors of Ypt1. As efficient interaction of Ypt1 with both effectors requires active GTP-bound Ypt1 [18,21], we analyzed which of these Ypt1 complexes is regulated by the Ypt1 GAP Gyp1. First, we asked whether Gyp1 influences the Ypt1-Atg11 interaction and thereby Atg11 PAS localization using fluorescence microscopy. Atg11 assembles with the Cvt complex, composed of prApe1 and Atg19 [13,70], and GTP-bound Ypt1 at the PAS, represented by a dot-like structure [14,18]. An *atg19*Δ strain was therefore used as a negative control, where Cherry-Atg11 is not properly recruited. In contrast, there were no significant differences in the number of Cherry-Atg11 dots/cell in WT and *gyp1*Δ cells (Figure 5(a,b)). The results indicate that formation of the Cvt complex and its assembly with Atg11 are independent of Gyp1.

Next, the PAS localization of GFP-tagged Atg1, the second effector of Ypt1 [21], was tested. The number of perivacuolar Atg1-GFP dots/cell, representing the PAS, was determined by fluorescence microscopy. We included again the *atg19*Δ strain as a negative control, where PAS assembly is abolished at an early step. The number of Atg1-GFP dots/cell increased significantly to approximately 40% in the *gyp1*Δ strain compared to the WT (Figure 5(c,d)). This enrichment of Atg1-GFP at the PAS in *gyp1*Δ cells indicates that PAS assembly is affected after Atg1 recruitment in the absence of Gyp1.

Deletion of the Ypt1 GAP stabilizes GTP-bound Ypt1, that preferably interacts with Atg1. We tested whether the accumulation of Atg1 at the PAS in *gyp1*Δ cells represents an enrichment of the Ypt1-Atg1 complex using a GFP-TRAP approach. Atg1-GFP was isolated under logarithmic growth conditions out of WT and *gyp1*Δ cells to determine the amount of co-precipitated endogenous Ypt1. Indeed, the amount of co-precipitated Ypt1 increased significantly in the *gyp1*Δ cells (203%) compared to the WT strain (Figure 5(e,f)). We confirmed, that disassembly of the Ypt1-Atg1 complex requires the GAP activity of Gyp1 by fluorescence microscopy of Atg1-GFP. We included Gyp1[AIM1] in the analysis, which caused no effect compared to Gyp1 cells. Otherwise, the number of perivacuolar Atg1-GFP dots/cell increased significantly to 47% in the Gyp1^{R343K} cells. Furthermore, the GAP

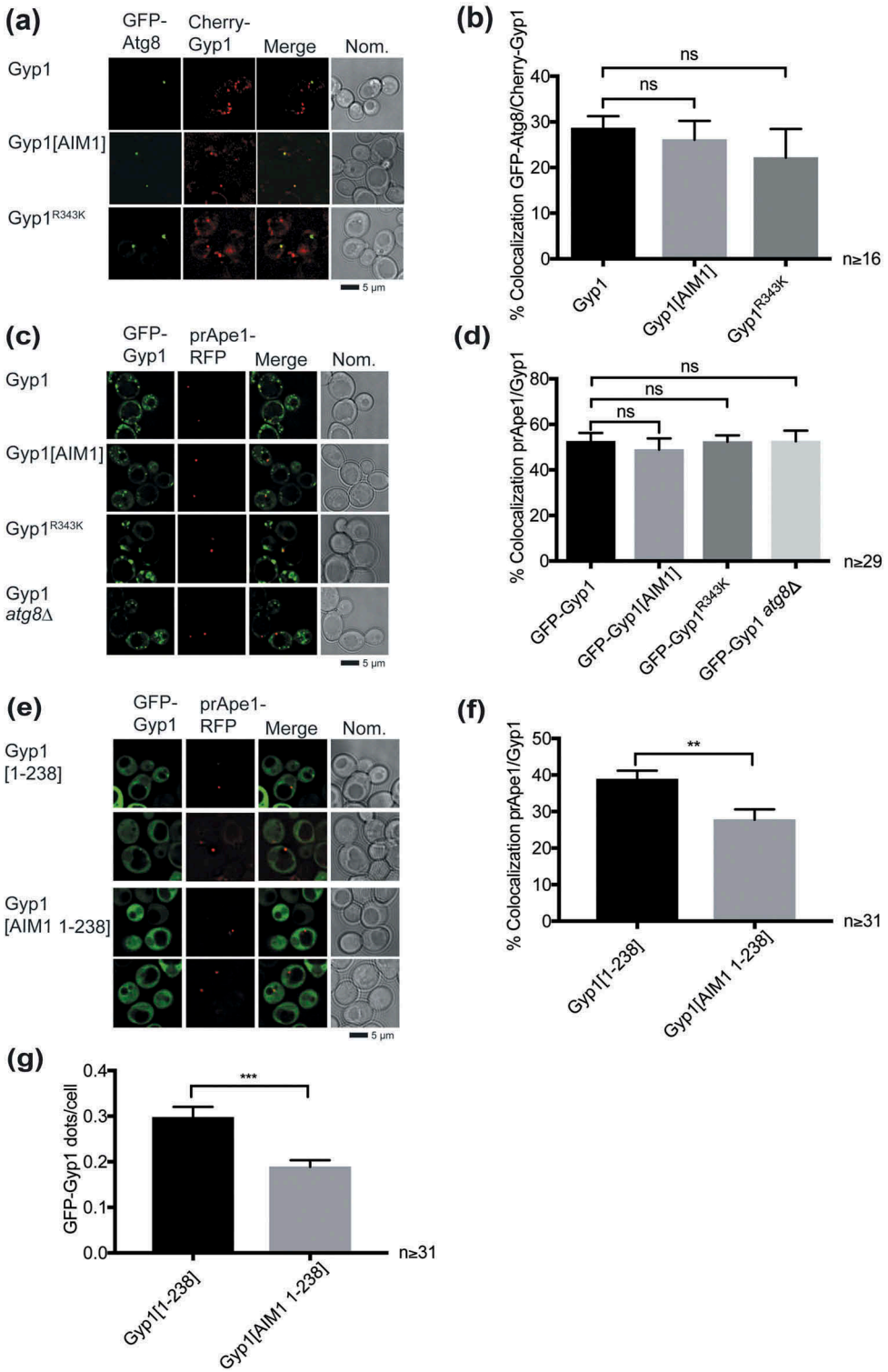

Figure 4. Gyp1 localizes to the Cvt-specific PAS. (a) Cherry-Gyp1, -Gyp1[AIM1] or -Gyp1^{R343K} and GFP-Atg8 were visualized by fluorescence microscopy in *gyp1*Δ *atg8*Δ cells grown to log phase. (b) Quantification of (a). The colocalization rate as the percentage of perivacuolar GFP-Atg8 PAS dots overlapping with Cherry-Gyp1 was determined: Gyp1 (28.62 ± 2.63%), Gyp1[AIM1] (26.10 ± 4.11%) and Gyp1^{R343K} (22.14 ± 6.30%). Dots/cell were analyzed from ≥16 different images/strain (≥440 cells/strain). (c) GFP-Gyp1, GFP-Gyp1[AIM1] or GFP-Gyp1^{R343K} and the PAS marker prApe1-RFP were visualized by fluorescence microscopy in *GYP1*-deleted cells grown to log phase. GFP-Gyp1 and prApe1-RFP were likewise analyzed in *atg8*Δ cells. (d) Quantification of (c). The colocalization rate as the percentage of perivacuolar prApe1-RFP PAS dots overlapping with GFP-Gyp1 was determined: GFP-Gyp1 (52.52 ± 3.74%), GFP-Gyp1[AIM1] (48.89 ± 4.95%), GFP-Gyp1^{R343K} (52.37 ± 2.83%) and GFP-Gyp1 in *atg8*Δ (52.50 ± 4.66%). Dots/cell were counted from ≥29 images/strain (≥370 cells). (e) GFP-Gyp1[1–238] and GFP-Gyp1[AIM1 1–238] and the PAS marker prApe1-RFP were visualized by fluorescence microscopy in *gyp1*Δ cells grown to log phase. (f) Quantification of the colocalization rate as the percentage of perivacuolar prApe1-RFP PAS dots overlapping with GFP-Gyp1 from (e). GFP-Gyp1[1–238] (38.48 ± 2.40%) and GFP-Gyp1[AIM1 1–238] (27.45 ± 3.71%). (g) Quantification of the number of GFP-Gyp1[1–238] dots per cell from (e): GFP-Gyp1[1–238] (0.30 ± 0.02) and GFP-Gyp1[AIM1 1–238] (0.19 ± 0.02). Dots/cell were counted from ≥31 images/strain (≥624 cells).

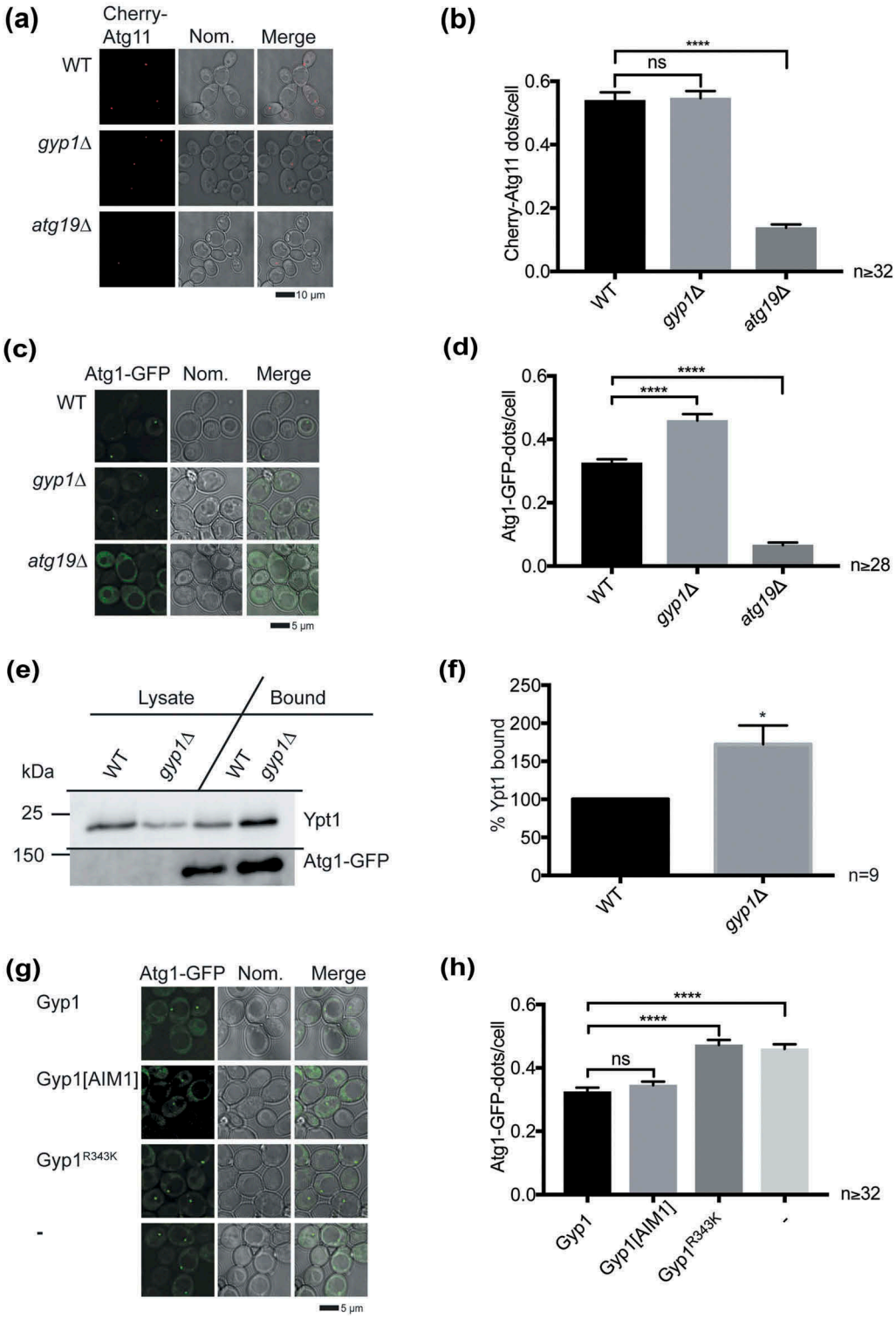

Figure 5. Gyp1 is required for efficient disassembly of the Ypt1-Atg1 complex. (a) Cherry-Atg11 was visualized by fluorescence microscopy in WT, *gyp1*Δ and *atg19*Δ cells (control) grown to log phase. (b) Quantification of (a). The number of Cherry-Atg11 dots/cell, was determined: WT (0.53 ± 0.03), *gyp1*Δ (0.55 ± 0.02) and *atg19*Δ (0.14 ± 0.01). ≥32 different images/strain were analyzed (≥753 cells/strain). (c) Atg1-GFP was expressed from the *ATG1* promoter and visualized by fluorescence microscopy in *atg1*Δ (WT), *gyp1*Δ *atg1*Δ and *atg19*Δ *atg1*Δ cells grown to log phase. (d) Quantification of (c). The number of perivacuolar Atg1-GFP dots/cell, representing the PAS, was determined in *atg1*Δ (0.33 ± 0.01), *gyp1*Δ *atg1*Δ (0.46 ± 0.02 dots/cell) and *atg19*Δ *atg1*Δ strains (0.07 ± 0.01), the latter used as a negative control. ≥28 different images/strain were analyzed (≥1027 cells/strain). (e) Atg1-GFP and endogenous Ypt1 were co-immunoprecipitated with a GFP-binding protein on beads out of *atg1*Δ (WT) and *atg1*Δ *gyp1*Δ cells grown to log phase. Immunoblots were probed with Ypt1 (top) or GFP antibodies (bottom). Molecular mass markers are in kDa. (f) Quantification of (e). The amount of Ypt1 bound to Atg1-GFP in *atg1*Δ cells (WT) was set to 100%. (g) Atg1-GFP and Gyp1, Gyp1[AIM1] or $Gyp1^{R343K}$ were expressed from the endogenous promoters in *atg1*Δ *gyp1*Δ cells grown to log phase. Atg1-GFP was visualized by fluorescence microscopy. (h) Quantification of (g). The number of perivacuolar Atg1-GFP dots/cell was determined: Gyp1 (0.32 ± 0.01), Gyp1[AIM1] (0.35 ± 0.01), $Gyp1^{R343K}$ (0.47 ± 0.02) and empty vector (0.46 ± 0.02). ≥32 different images/strain were analyzed (≥1190 cells/strain).

mutant caused the same effect as the strain lacking Gyp1 (Figure 5(g,h)). Taken together, these results show, that the Cvt pathway requires Gyp1 as a Ypt1 GAP for efficient disassembly of the Ypt1-Atg1 complex.

Proper recruitment of Atg14 and Atg8 to the PAS requires Gyp1

Recruitment of the Atg14-containing class III PtdIns 3-kinase complex I is dependent on the Atg1 kinase complex and Atg9 [39,40,71,72]. We tested whether efficient disassembly of the Ypt1-Atg1 complex by Gyp1 is required for proper Atg14 localization to the PAS. The number of perivacuolar Atg14-GFP dots/cell, representing the PAS, was determined under logarithmic growth conditions. In the *atg9*Δ strain, used as a negative control, the number of Atg14-GFP dots/cell decreased significantly to 44%. The number of Atg14-GFP dots/cell was further significantly reduced to 65% in *gyp1*Δ cells compared to the WT (Figure 6(a,b)). This result indicates that inactivation of Ypt1 by Gyp1, and thereby efficient disassembly of the Ypt1-Atg1 complex, is a prerequisite for proper Atg14 recruitment and PtdIns3P production at the PAS. Thereby, the critical step from nucleation to phagophore elongation is initiated.

We further analyzed the localization of the Gyp1 interaction partner Atg8 by fluorescence microscopy. Under nutrient-rich conditions the late PAS component Atg8 is recruited in a PtdIns3P-dependent manner via Atg21 to the PAS [42]. In *atg21*Δ control cells the number of GFP-Atg8 dots/cell decreased significantly to 38%. Again, likely due to the reduced amount of PtdIns3P at the PAS, the number of GFP-Atg8 dots/cell decreased significantly to 73% in the *gyp1*Δ strain compared to the WT (Figure 6(c,d)). We also analyzed the influence of Gyp1-Atg8 interaction and the Gyp1 GAP activity. Compared to cells containing Gyp1, the number of GFP-Atg8 dots/cell decreased significantly in cells lacking Gyp1 and containing the Gyp1^{R343K} GAP mutant, but there was no significant change in the number of GFP-Atg8 dots/cell in the presence of Gyp1[AIM1] (Figure 6(e,f)). This result is highly interesting as it indicates that recruitment of GFP-Atg8 to the PAS, represented by the number of perivacuolar GFP-Atg8 dots/cell, is dependent on the GAP activity of Gyp1 due to inefficient disassembly of the Ypt1-Atg1 complex, but not on the Gyp1 AIM1.

Efficient interaction of Atg8 with cargo receptors requires the Gyp1 AIM1

Gyp1[AIM1] reduced the mitophagy rate (Figure 3(g,h)) although it caused no defect in Atg1-GFP and GFP-Atg8 localization to the PAS (Figure 5(g,h); 6(e,f)). What could be the role of the Gyp1 AIM1 after GFP-Atg8 recruitment to the PAS that affects at least the mitophagy rate? Following recruitment and lipidation, Atg8–PE must be efficiently directed to the different Atg8–PE functional complexes, including the cargo complex on the inside of the forming Cvt vesicles or the Atg12–Atg5-Atg16 coat-like structure on the outside of phagophores [11,12,50]. We analyzed whether the Atg8-cargo receptor complexes form efficiently in cells containing Gyp1[AIM1]. Flag-tagged Atg8 and the mitophagy receptor GFP-Atg32 were co-immunoprecipitated out of cells either containing Gyp1, Gyp1[AIM1], Gyp1^{R343K} or lacking Gyp1. The percentage of Flag-tagged Atg8 that co-precipitated with GFP-Atg32 decreased significantly in cells containing Gyp1[AIM1] (69%) and Gyp1^{R343K} (50%) compared to the cells containing Gyp1. The percentage of co-isolated Flag-tagged Atg8 was also clearly reduced in cells lacking Gyp1 (64%; Figure 7(a,b)). Next, we extended our analysis on the Cvt cargo complex to confirm the role of the Gyp1 AIM1. Thus, we co-isolated Flag-tagged Atg8 and the Cvt receptor Atg19-HA out of cells either containing Gyp1, Gyp1[AIM1], or Gyp1^{R343K}, or cells lacking Gyp1. Indeed, the percentage of Flag-tagged Atg8 that co-precipitated with Atg19-HA decreased significantly in cells containing Gyp1[AIM1] (56%) and Gyp1^{R343K} (54%) compared to cells containing Gyp1. The percentage of co-isolated Flag-tagged Atg8 decreased further in cells lacking Gyp1 (25%; Figure 7(c,d)). The decreased amount of cargo receptor-Atg8–PE complexes in cells containing Gyp1^{R343K} or lacking Gyp1 are likely caused by the recruitment defect of GFP-Atg8 to the PAS (Figure 6(e,f)). In contrast, the Gyp1 AIM1 is not required for recruitment of GFP-Atg8 to the PAS (Figure 6(e,f)) but in a later step for efficient formation of the cargo receptor-Atg8–PE complexes. Thereby, we could show that Gyp1 is required for 2 separate steps of PAS assembly during selective autophagy. Gyp1 acts as a GAP of Ypt1 to mediate efficient disassembly of the Ypt1-Atg1 complex and later as an Atg8 interaction partner.

The precise regulation of complex assembly and disassembly is a prerequisite for proper PAS organization, but the mechanisms are mostly unclear. The Cvt pathway serves as a prototype for selective autophagy in yeast [8]. Therefore, we propose a model for Gyp1 in regulating Ypt1 activity and dynamic PAS assembly under nutrient-rich conditions (Figure 8). The Cvt complex (prApe1 and Atg19) assembles with Atg11, Atg9 vesicles as an initial membrane source, Atg1 and Ypt1. Thereby, Atg1 interacts with GTP-bound Ypt1 [21]. The Gyp1 GAP activity leads to GTP hydrolysis and thereby efficient disassembly of the Ypt1-Atg1 complex. Thus, Gyp1 sets the stage for efficient Atg14 recruitment and PtdIns3P production at the PAS, and facilitates the critical step from nucleation to elongation of the phagophore. PtdIns3P is bound by Atg21 that recruits Atg8 and Atg16, leading to Atg8 lipidation [42]. Efficient formation of the cargo receptor-Atg8–PE complexes then requires AIM-dependent binding of Gyp1 to Atg8–PE.

Discussion

Selective autophagy requires fine-tuning by the GAP Gyp1

Rab GTPases are major regulators of vesicle trafficking, and their role in autophagy has attracted increasing attention over the years [73]. Their activity is controlled by GEFs, GAPs and GDP dissociation inhibitors [32]. We show that the GAP Gyp1 is involved in dynamic complex disassembly during selective autophagic variants (Figure 8). Ypt1 regulation by Gyp1 is highly important because both *GYP1* overexpression, which enriches GDP-bound Ypt1, and deletion of *GYP1*, which stabilizes GTP-bound Ypt1, impeded the Cvt pathway (Figure 3(a,b), S4E-F). Furthermore, Ypt1^{Q67L}, dominantly in

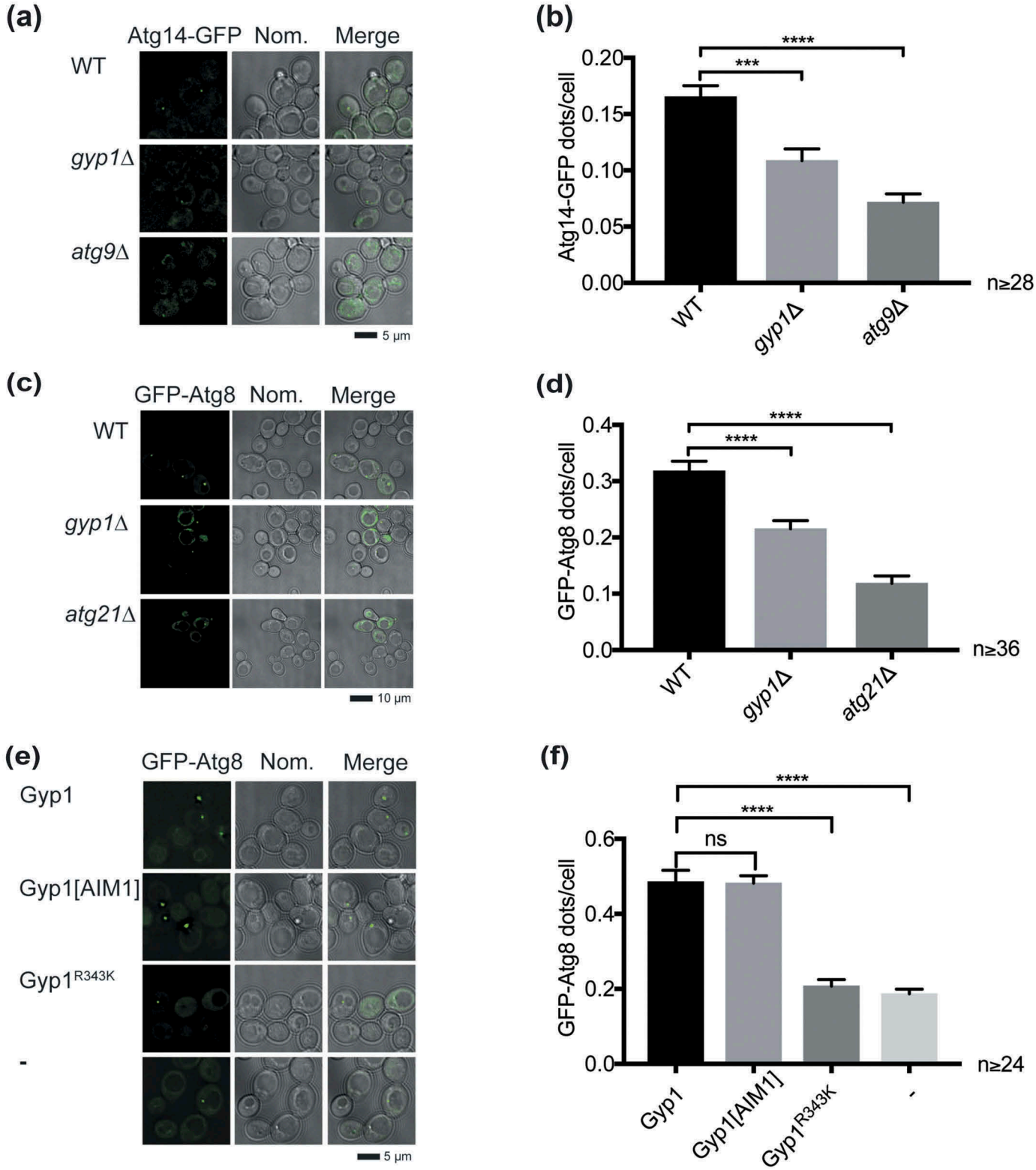

Figure 6. Efficient PAS localization of Atg14-GFP and GFP-Atg8 requires Gyp1. (a) *ATG14* was chromosomally tagged with *GFP* and visualized by fluorescence microscopy in WT, *gyp1*Δ and *atg9*Δ cells grown to log phase. (b) Quantification of (a). The number of perivacuolar Atg14-GFP dots/cell, representing the PAS, was determined: WT (0.17 ± 0.01 dots/cell), *gyp1*Δ (0.11 ± 0.01) and *atg9*Δ (0.07 ± 0.01), the latter was used as a negative control. ≥28 different images/strain were analyzed (≥636 cells/strain). (c) GFP-Atg8 was expressed from its own promoter and visualized by fluorescence microscopy in WT, *gyp1*Δ and *atg21*Δ cells (control) grown to log phase. (d) Quantification of (c): WT (0.30 ± 0.02), *gyp1*Δ (0.22 ± 0.02) and *atg21*Δ (0.12 ± 0.01) cells. ≥36 different images/strain were analyzed (≥1051 cells/strain). (e) GFP-Atg8 was visualized by fluorescence microscopy in *gyp1*Δ *atg8*Δ cells grown to log phase expressing Gyp1, Gyp1[AIM1] or $Gyp1^{R343K}$ or empty vector (-). (f) Quantification of (e). The number of perivacuolar GFP-Atg8 dots/cell was determined: Gyp1 (0.49 ± 0.03), Gyp1[AIM1] (0.48 ± 0.02), $Gyp1^{R343K}$ (0.21 ± 0.02) and empty vector (0.19 ± 0.01). ≥24 different images/strain were analyzed (≥689 cells/strain).

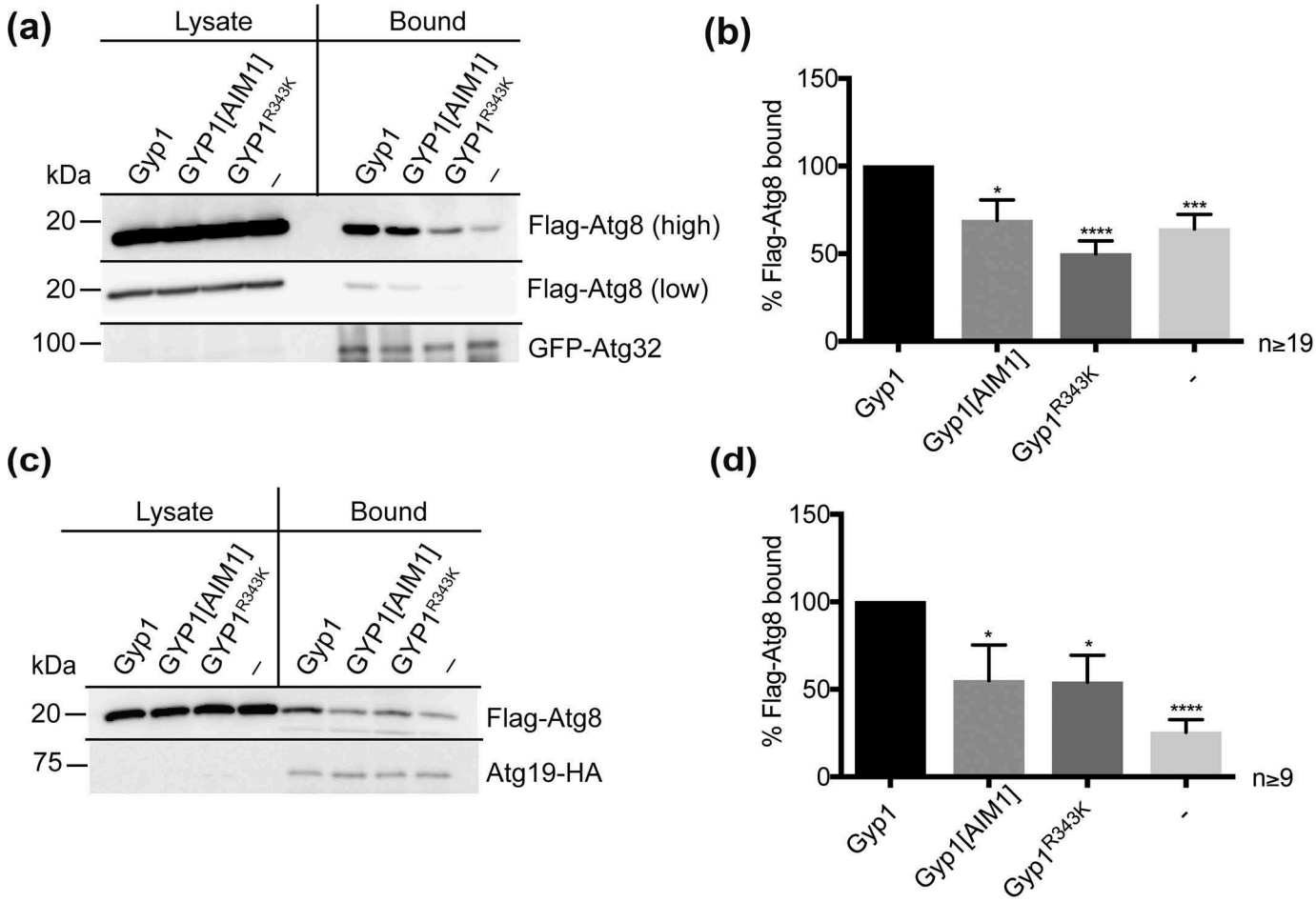

Figure 7. Efficient interaction of Atg8 with cargo receptors requires the Gyp1 AIM1 motif. (a) Flag-Atg8 and GFP-Atg32 were co-immunoprecipitated with GFP beads out of *gyp1*Δ *atg8*Δ *atg32*Δ cells grown to log phase expressing Gyp1, Gyp1[AIM1], Gyp1^{R343K} or empty vector (-). Immunoblots were probed with Flag antibody (top), shown after longer (high) or shorter (low) exposure, or GFP antibody (bottom). (b) Quantification of (a). The ratio of Flag-Atg8 bound to GFP-Atg32 in Gyp1 cells was set to 100%. (c) Flag-Atg8 and Atg19-HA were co-immunoprecipitated with HA-agarose out of *gyp1*Δ *atg8*Δ Atg19-HA cells in log phase expressing Gyp1, Gyp1[AIM1], Gyp1^{R343K} or empty vector (-). Immunoblots were probed with Flag (top) or HA antibodies (bottom). (d) Quantification of (c). The amount of Flag-Atg8 bound to Atg19-HA in Gyp1 cells was set to 100%.

its GTP-bound form, also affected the Cvt pathway (Figure S4C-D), although another study reported a slight elevation in Pho8Δ60 activity also under basal conditions when Ypt1^{Q67L} was overexpressed under control of the *GAL1* promoter [32]. Together with the conservation of the Ypt1/RAB1-Atg1/ULK1 interaction in mammals our findings emphasize the importance of Gyp1 for autophagy [21]. In addition, highly conserved Gyp1 orthologs exist in various species. The RABGAP domain of a human ortholog TBC1D22A (accession number AL096779) shares 48% identity with Gyp1 (excluding a non-conserved loop region in Gyp1) [34]. Therefore, it is tempting to speculate that the orthologs of Gyp1 are also required for selective autophagy.

The GTP hydrolysis of Ypt1 is increased 54-fold in the presence of saturating amounts of Ypt1-GAP activity [62], but residual GTP hydrolysis in the absence of Ypt1-GAP activity might explain the partial phenotypes of the GAP deletion strains. Even Ypt1^{Q67L}, predominantly in its GTP-bound form, is responsive to the GAP activity, although its stimulated rate is much slower [62]. In addition, the different GAPs have the potential to compensate for each other as shown for Gyp5 and Gyp8 in the absence of Gyp1 (Figure 3(a,b)). We can also not fully exclude yet that additional GAPs contribute to the inactivation of Ypt1 at the PAS.

Without providing mechanistic insights, another study also showed a reduced autophagic rate for *GYP1* deleted cells upon starvation [36]. This seems to be in line with a general role of Ypt1 in autophagy [18,21,22]. However, we could neither detect an effect on prApe1 maturation under starvation conditions in different yeast backgrounds nor a significant defect in GFP-Atg 8 or Pgk1-GFP processing even after shorter times of starvation (Figure 3(e,f), Figure S4A-B, Figure S5). Otherwise, the Ypt1 GEF component Trs85 is strictly required for selective autophagy, but to what extent Trs85 is required for non-selective macroautophagy is still under debate [18,22,27]. Most recently it has been proposed that only additional deletion of *TRS33* abolishes non-selective autophagy [28].

Most recently, a role of the Trs85-containing TRAPPIII in Ypt1 activation during ER-Golgi transport has also been proposed [29]. This is in line with studies showing that *trs85*Δ cells are impaired in both ER-Golgi trafficking and endocytic recycling [23,74,75]. A function of Gyp1 in endosomal recycling and as a Ypt1 GAP at the Golgi has also been proposed [33–35]. In our hands the *gyp1*Δ strain secreted only minimal

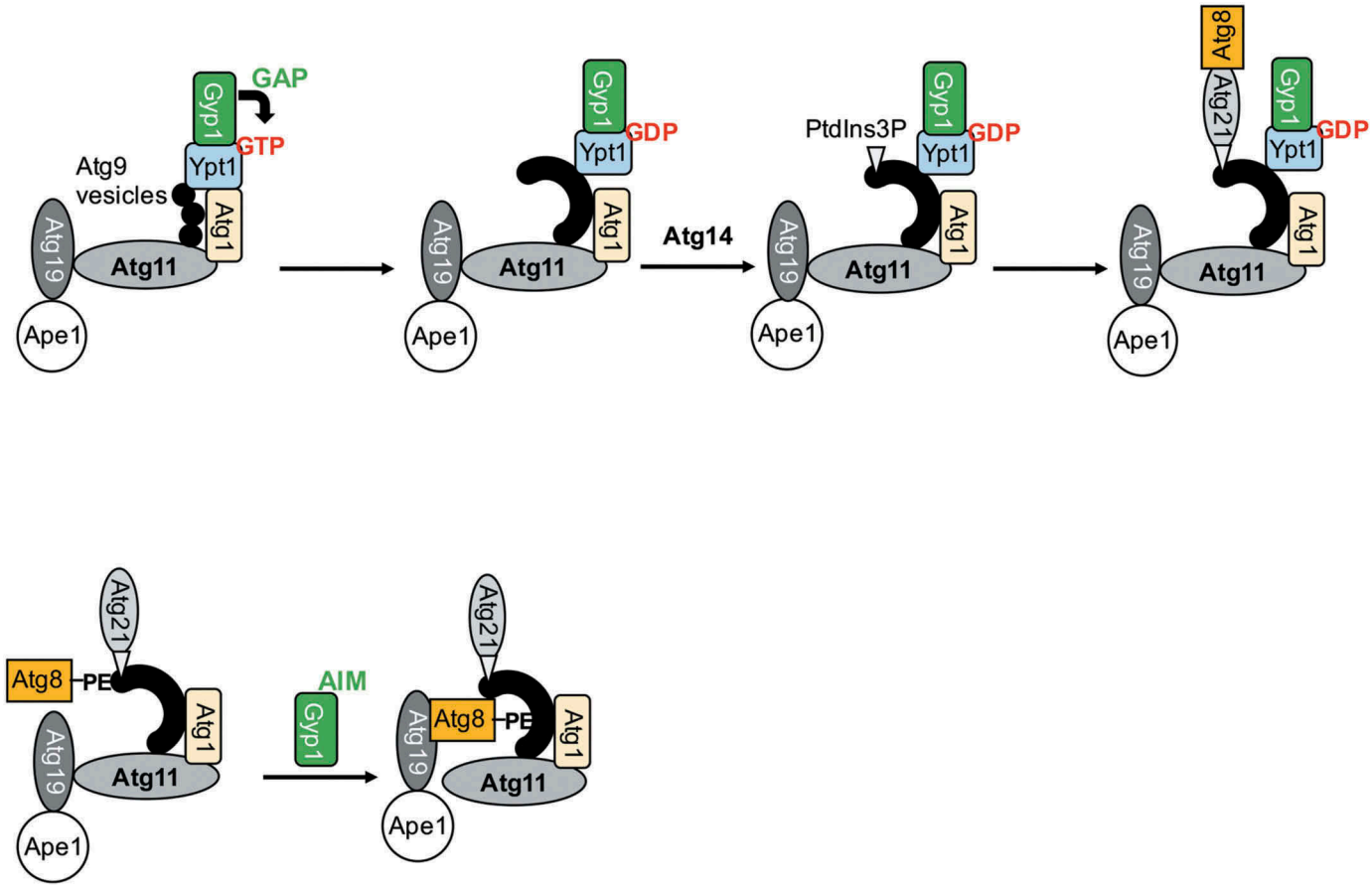

Figure 8. Current model for Gyp1 function. Efficient selective autophagy requires Gyp1 at 2 different steps. First, the Gyp1 GAP activity is required for efficient disassembly of the Ypt1-Atg1 complex, and then Gyp1 AIM1 is required for efficient formation of the cargo receptor-Atg8–PE complexes. Model is detailed in the text.

amounts of Prc1/CPY (Figure S6A). This mild Prc1/CPY secretion phenotype was not increased by additional deletion of *GYP5* and *GYP8*, which significantly increased the prApe1 maturation defect (Figure 3(a,b)). Normal Prc1/CPY maturation in *gyp1*Δ and *gyp1*Δ *gyp5*Δ *gyp8*Δ cells (Figure S6B-C) ruled out the possibility that disturbed vacuolar proteolysis caused the prApe1 maturation defect. Trs85 and Gyp1 might act on Ypt1 in the secretory pathway and autophagy. The direct AIM-dependent interaction of Gyp1 with Atg8, its localization to the PAS and proper PAS assembly until recruitment of Atg1 (Figure 1–2; Figure 4–6) clearly show an autophagy specific function and argue against an indirect effect of the *GYP1* deletion on selective autophagy [66,67].

Gyp1 is required for efficient disassembly of the Ypt1-Atg1 complex

We analyzed the localization of different Atg proteins in *GYP1* deleted cells and identified the steps during PAS assembly that require Gyp1 under nutrient-rich conditions, as indicated in our model (Figure 8). Atg11 assembly at the PAS occurred normally in *gyp1*Δ cells, represented by one single perivacuolar Cherry-Atg11 dot/cell (Figure 5(a,b)). In contrast, *ypt1-1* (T40K) cells show a disturbed recruitment of Atg11 to the PAS, and thus multiple GFP-Atg11 dots/cell, due to a defect in interaction of Ypt1 with its effector Atg11 [18,22]. We further showed, that inefficient disassembly of the Ypt1-Atg1 complex caused significant enrichment of Atg1-GFP at the PAS in cells lacking Gyp1 (Figure 5(c–f), Figure 8). The *ypt1-2* mutant is inactive due to a defect in GTP binding [76], and showed no Atg1-GFP enrichment under nutrient-rich conditions [21]. Most likely GTP-dependent formation of the Ypt1-Atg1 complex is affected in this mutant, avoiding accumulation of Atg1.

Formation of the Ypt1-Atg1 complex might be differently regulated under nutrient-rich conditions and upon starvation or rapamycin treatment as described for the activation of Atg1. Atg13 is hyperphosphorylated under nutrient-rich conditions, decreasing the Atg1-Atg13 interaction [77–79]. Therefore, Atg1 activation additionally requires cargo-bound Atg11 to cluster Atg1 [15,16], and the Ypt1-Atg1 complex needs fine-tuning by Gyp1 under nutrient-rich conditions. After Ypt1-Atg1 complex disassembly, the described AIM-dependent interaction of Atg1 and Atg8 might lead to association of Atg1 with autophagosomes and downregulate the Atg1 kinase complex and/or facilitate membrane expansion [53,80].

Gyp1 has a GAP-independent function as an Atg8 interaction partner

Gyp1 functions not only as a GAP for Ypt1 but its AIM-dependent interaction with Atg8 facilitates the formation of

Atg8-cargo complexes required during selective autophagy (Figure 7). Various TBC domain-containing RAB GAPs have been identified that bind directly to Atg8-family protein modifiers and colocalize with LC3-positive autophagic membranes [81]. In addition, Gyp1 is not the only TBC domain-containing protein with a GAP-independent function. The mammalian protein TBC1D14 exerts its dominant negative effect on autophagy by interaction with the TRAPP complex [59,60].

Besides the AIM-binding site, the Gyp1-Atg8 interaction also slightly required the Atg8 NHD (Figure 1(c,d)), probably to stabilize the interaction. Gyp1[AIM3] only increased its coprecipitation with GFP-Atg8 out of yeast cells (Figure 2(a,b), (d,e)). In whole cells, the AIM3 mutation might affect binding of Gyp1 to another interaction partner and thereby increase the pool of free Gyp1 available for interaction with Atg8, whereas this is not detectable upon reconstitution of the complexes using isolated GST-Atg8.

Although Gyp1[AIM1] strongly affected binding of Gyp1 to Atg8 (Figure 2(a–e)) in binding assays, it only reduced the mitophagic rate and caused no prApe1 maturation defect in living cells (Figure 3(c,d); (g,h)). Therefore, the GAP activity seems to be the Gyp1 function dominantly required for the Cvt pathway. Furthermore, we measure on a high background of Ape1 in the deletion strains. Therefore, a reduced Cvt vesicle biogenesis in the Gyp1[AIM1] mutant might be masked especially by degradation of prApe1 as large oligomers, leading to overestimation of the prApe1 maturation rate [61]. However, additional AIMs in Gyp1 could also mask the phenotype or cause the partial mitophagy defect. The Cvt receptor Atg19, for example, contains multiple cryptic AIMs that contribute to the Atg19-Atg8 interaction [82]. We mutated additional potential AIMs in Gyp1, but instability of the mutated proteins precluded their analysis (Figure S2B). We showed that AIM1 might be additionally required for localization of Gyp1 at the PAS *in vivo* using a truncated version of Gyp1 lacking the TBC domain, that masked this phenotype (Figure 4(e–g)), although the main PAS localization motif resides in the C-terminal part of Gyp1 containing the TBC domain (Figure 4(a–d)). The supplemental Gyp1[1–238] PAS recruitment (Figure 4(e–g)) by interaction with Atg8 could represent a reinforcing feedback loop. Atg8 could donate Gyp1 to the Ypt1 complex to enforce disassembly of the Ypt1-Atg1 complex and thereby its own recruitment. It might be also possible, that the AIM motif is masked in the presence of the TBC domain. A conformational change could be induced after recruitment of Gyp1 to the PAS or upon deletion of the TBC domain, allowing access to AIM1. Otherwise, GFP-Gyp1[1–238] caused a strong cytosolic pool (Figure 4(e), Figure S7A), that is absent in cells containing the full-length GFP-Gyp1 constructs. Therefore, Atg8 could also recruit GFP-Gyp1[1–238] from this cytosolic pool to the PAS, that is absent under physiological conditions. Nevertheless, AIM1 of Gyp1 is required for efficient interaction of Atg8 with the cargo receptors Atg19 and Atg32 (Figure 7(a–d)) as depicted in our model (Figure 8). Therefore, we propose that the Gyp1-Atg8 interaction is required for spatial segregation of Atg8–PE from the lipidation complex to the cargo complexes during selective autophagy.

Our findings elucidate the molecular mechanisms of complex disassembly during phagophore formation and suggest potential dual functions of GAPs in cellular vesicle trafficking independent of their role as Rab GTPase regulators.

Materials and methods

Plasmids

The plasmids used in this study can be found in Table 1. Genes have been cloned with the endogenous promoter if not indicated otherwise. *GYP1-6xHA* has been amplified with the endogenous promoter from chromosomal DNA and inserted with SacI-HindIII into pRS316 for pRS316-Gyp1-6xHA. For pRS315-Gyp1-6xHA, *GYP1-6xHA* has been amplified with the endogenous promoter from chromosomal DNA and inserted with SacI-SalI into pRS315. *MET25p*-Cherry-Gyp1 was constructed by PCR amplification of *GYP1* from chromosomal DNA and inserted via BamHI-SalI into *MET25p*-Cherry (pUG34 derivate). This construct derived from pMET25-Cherry (pUG36 derivate) [42] by replacing GFP with Cherry (SacI-Spe1). After mutagenesis of AIM1 the inserts were isolated and ligated into pUG34 to yield the pUG34-Gyp1 constructs. *GYP1* with its promoter and terminator was amplified by PCR from chromosomal DNA and inserted via SacI-SalI into pRS315 for pRS315-Gyp1. After mutagenesis of AIM1 and R343K all inserts have been isolated again via SacI-SalI and ligated with pRS316 to yield the pRS316-Gyp1 constructs. Mutagenesis of the indicated amino acids has been done with QuikChange Lightning Site-Directed Mutagenesis Kit (Agilent Technologies, 210519) and corresponding primers.

pUG36-mCherry-Atg11 was constructed by amplification of *ATG11* from chromosomal DNA and ligation via BamHI-XhoI into pMET25-Cherry [42].

For the pPROExHtb-Gyp1 constructs the inserts have been isolated from *MET25p*-Cherry-Gyp1 variants and ligated into pPROExHtb via BamHI-SalI.

2xFlag-ATG8 was amplified by overlapping extension PCR and ligated via EcoRI and XhoI into pRS313. *ATG32* was amplified by PCR from chromosomal DNA and ligated into XhoI-EcoRI of pUG36.

For mito-GFP the pre-sequence of the *N. crassa* subunit 9 (atp-9/Su9) of the F_1F_o ATPase fused to mouse DHFR, dihydrofolate reductase was amplified by PCR and inserted with BamH1-EcoR1 into pUG23.

Yeast strains

The yeast strains used in this study can be found in Table 2. All strains are in the WCG4a background if not indicated otherwise. The indicated knockouts have been done according to previous reports [83,84] using pFa6a-natNT2, pFa6a-hphNT1, pFa6a-His3MX6 or pFa6a-KaMX6 as template. Tagging of the indicated genes with GFP has been also done according to a previous report [84] using pFA6a-GFP(S65T)-HIS3MX6 as template. The integration of the *GPD1* promoter has also been done according to a previous report [83] using pYM-N16 as template. Tagging of the indicated genes with 6xHA has been done using pYM17 as template following the protocol provided previously [83].

Table 1. Plasmids used in this study.

Name	Characteristics	Source
GST-Atg8	pGEX4T3-Atg8	[56]
GST	pGEX4T3	GE Healthcare, 28-9545-52
GST-Atg8_L50A	pGEX4T3-Atg8_L50A	[56]
GST-Atg8_FK	pGEX4T3-Atg8_F5G K6G	[56]
GST-Atg8_ST	pGEX4T3-Atg8_S3A T4A	[56]
His_6_Gyp1	pPROExHtb-Gyp1	This study
His_6_Gyp1_AIM1	pPROExHtb-Gyp1_ W160A V164A	This study
His_6_Gyp1_R343K	pPROExHtb-Gyp1_R343K	This study
pRS316-Gyp1-6xHA	pRS316-Gyp1-6xHA	This study
pRS316-Gyp1_AIM1-6xHA	pRS316-Gyp1_ W160A V164A −6xHA	This study
pRS316-Gyp1_AIM2-6xHA	pRS316-Gyp1_ F426A L429A −6xHA	This study
pRS316-Gyp1_AIM3-6xHA	pRS316-Gyp1_ W625A L628A-6xHA	This study
pRS316-Gyp1_R343K-6xHA	pRS316-Gyp1_R343K-6xHA	This study
pRS316	CEN, URA3	[88]
GAL_GFP-Atg8	pYES2-GFP-Atg8	[89]
GAL_GFP-Atg8_L50A	pYES2-GFP-Atg8_L50A	[89]
GAL_GFP-Atg8_Y49A	pYES2-GFP-Atg8_Y49A	[89]
GAL_GFP-Atg8_FK	pYES2-GFP-Atg8_ F5G K6G	[42]
GAL_GFP-Atg8_ST	pYES2-GFP-Atg8_ S3A T4A	[42]
GAL_GFP	pYes2	Invitrogen, V82520
pRS315-Gyp1-6xHA	pRS315-Gyp1-6xHA	This study
pRS315-Gyp1_AIM1-6xHA	pRS315-Gyp1_ W160A V164A −6xHA	This study
pRS315-Gyp1_AIM2-6xHA	pRS315-Gyp1_ F426A L429A −6xHA	This study
pRS315-Gyp1_AIM3-6xHA	pRS315-Gyp1_ W625A L628A-6xHA	This study
pRS315-Gyp1_AIM4-6xHA	pRS315-Gyp1_ F258A I261A-6xHA	This study
pRS315-Gyp1_AIM5-6xHA	pRS315-Gyp1_ W278A I281A-6xHA	This study
pRS315-Gyp1_AIM6-6xHA	pRS315-Gyp1_ W290A L293A-6xHA	This study
pRS315-Gyp1_AIM7-6xHA	pRS315-Gyp1_ W334A I337A-6xHA	This study
pRS315-Gyp1_R343K-6xHA	pRS315-Gyp1_ R343K-6xHA	This study
pRS315	CEN, LEU2	[88]
GFP-Atg8	pRS316-GFP-Atg8	[88]
GFP-Atg8	pRS315-GFP-Atg8	[56]
GFP-Atg8_L50A	pRS315-GFP-Atg8_L50A	[56]
GFP	pRS315-GFP (*ATG8* promoter)	This study
2xFlag-Atg8	pRS313-2xFlag-Atg8	This study
mito-GFP	*MET25p*-atp-9/Su9-DHFR-GFP (pUG23)	This study
pRS315-Gyp1	pRS315-Gyp1	This study
pRS315-Gyp1_AIM1	pRS315-Gyp1_ W160A V164A	This study
pRS315-Gyp1_R343K	pRS315-Gyp1_R343K	This study
pRS316-Gyp1	pRS316-Gyp1	This study
pRS316-Gyp1_AIM1	pRS316-Gyp1_ W160A V164A	This study
pRS316-Gyp1_R343K	pRS316-Gyp1_R343K	This study
GFP-Gyp1	pUG34-Gyp1; MET25	This study
GFP-Gyp1_AIM1	pUG34-Gyp1_ W160A V164A; MET25	This study
Cherry-Gyp1	*MET25p*-mCherry_Gyp1 (HIS)	This study
Cherry-Gyp1_AIM1	*MET25p*-mCherry_Gyp1_W160A V164A (HIS)	This study
Cherry-Gyp1_R343K	*MET25p*-mCherry_Gyp1_R343K (HIS)	This study
Ape1-RFP	pRS316-Ape1-RFP	[26]
Cherry-Atg11	*MET25p*-mCherry-Atg11 (URA3)	This study
Atg1-GFP	pRS315-Atg1-GFP	[80]
GFP-Atg32	*MET25p*-GFP-Atg32 (URA)	This study

Antibodies

Anti-Atg8 antibody was described previously [85].Generation of anti-Ape1 was also described previously [86]. The other antibodies were purchased from different companies: Anti-GFP antibody (Roche,11814460001), anti-Pgk1 (Invitrogen, A6457), anti-Prc1/carboxypeptidase Y (CPY; Molecular Probes, A6428), anti-Flag (Sigma, F1804), anti-HA (Santa Cruz Biotechnology, sc-7392), HisProbe^{TM}-HRP (Thermo Fisher Scientific, 15165), horseradish peroxidase-conjugated goat anti-rabbit (Life Technologies, G21234) and horseradish peroxidase-conjugated goat anti-mouse (Dianova, 115-035-166).

Isolation of GST-Atg8 and GST

The isolation protocol has been described previously [42].

Table 2. Yeast strains used in this study.

Name	Genotype	Source
WCG4a	Mat alpha; *ura3 his3-11,15 leu2-3,112,26*	[90]
atg1Δ	*atg1::kanMX6*	[91]
gyp1Δ	*gyp1::hphNT1*	This study
gyp5Δ	*gyp5::natNT2*	This study
gyp8Δ	*gyp8::kanMX6*	This study
gyp1Δ gyp5Δ	*gyp1::hphNT1 gyp5::natNT2*	This study
gyp1Δ gyp8Δ	*gyp1::hphNT1 gyp8::kanMX6*	This study
gyp5Δ gyp8Δ	*gyp5::natNT2 gyp8::kanMX6*	This study
gyp1Δ gyp5Δ gyp8Δ	*gyp1::hphNT1 gyp5::natNT2 gyp8::kanMX6*	This study
Gyp1-6xHA	*GYP1-6xHA::natNT2*	This study
Gyp5-6xHA	*GYP5-6xHA::natNT2*	This study
Gyp8-6xHA	*GYP8-6xHA::natNT2*	This study
Gyp1-6xHA *atg8Δ*	*GYP1-6xHA::natNT2 atg8Δ::kanMX6*	This study
gyp1Δ gyp8Δ	*gyp1::hphNT1 atg8::kanMX6*	This study
Atg14-GFP	*ATG14-GFP::His3MX6*	This study
Atg14-GFP *gyp1Δ*	*ATG14-GFP::His3MX6 gyp1::hphNT1*	This study
Atg14-GFP *atg9Δ*	*ATG14-GFP::His3MX6 atg9::hphNT1*	This study
atg19Δ atg1Δ	*atg19::kanMX6 atg1::natNT2*	This study
gyp1Δ atg1Δ	*gyp1::hphNT1 atg1::His3MX6*	This study
atg1Δ	*atg1::His3MX6*	This study
atg19Δ	*atg19::kanMX6*	[85]
GPD-Gyp1	*natNT2::GPD-3xHA-GYP1*	This study
GPD-Gyp7	*natNT2::GPD-3xHA-GYP7*	This study
atg21Δ	*atg21::kanMX6*	[64]
atg8Δ gyp1Δ Atg19-6xHA	*atg8::kanMX6 gyp1::hphNT1 Atg19-6xHA::nanTN2*	This study
pep4Δ atg32Δ gyp1Δ	*pep4::kanMX6 atg32::nanNT2 gyp1::hphNT1*	This study
BY4741	Mata; *his3Δ1, leu2Δ0, met15Δ0, ura3Δ0*	Euroscarf
BY4741 *gyp1Δ*	*gyp1::kanMX6*	Euroscarf (Y01846)
BY4741 *gyp5Δ*	*gyp5::natNT2*	This study
BY4741 *gyp8Δ*	*gyp5::hphNT1*	This study
BY4741 *gyp1Δ gyp5Δ gyp8Δ*	*gyp1::kanMX6 gyp5::natNT2 gyp8::hphNT1*	This study
BY4741 *vps21Δ*	*vps21::kanMX6*	Euroscarf (Y01865)
WCG4a *pep4Δ*	*pep4::kanMX6*	[90]

Isolation of His_6-Gyp1

E. coli cells were grown to an OD_{600} of 0.5–0.8, induced with 0.1 mM isopropyl-β-D-thiogalactopyranoside (Roth, 2316.3) for 4–5 h at 30°C, harvested, snap-frozen, and stored at −80°C. Cells were lysed in ice-cold 1x PBS, pH 7.4 (140 mM NaCl [Roth, 3957.5], 2.7 mM KCl [Roth, 6781.3], 10 mM Na_2HPO_4 [Roth, 4984.1], 1.8 mM KH_2PO_4 [Roth, 3904.1]) containing protease inhibitor mixture (Sigma, P8465), 2 mM $MgCl_2$ (Roth, 2189.1), benzonase (Sigma, E1014-25KU), and 1% Triton X-100 (Roth, 3051.2). Supernatants from lysed cells (15 min, 8000 x g at 4°C) were applied to Ni-NTA Sepharose (QUIAGEN, 151028822) for 30–50 min at 4°C. Elution followed the manufacturer's protocol. Protein concentration was determined using the Bradford method, and purity verified by SDS-PAGE using Coomassie Brilliant Blue staining.

Affinity isolation experiments with yeast crude extracts

Eighty OD_{600} units of the indicated strains grown to logarithmic phase were glass-bead lysed in cold binding buffer (BB1: 1x PBS, pH 7.4, 5 mM $MgCl_2$, 0.5% Triton X-100, and protease inhibitors [Complete; Roche, 05056489001]). 4 OD_{600} of cleared lysate was removed (Lysate), and the rest incubated for 2–4 h at 4°C with beads carrying equal amounts of GST fusions. Beads were washed 4 times with BB1. Beads were then resuspended in 50 µl Laemmli sample buffer (Bound). For immunoblotting, 10 µl of samples were used. The lysates correspond to 4% of the bound fraction. For immunoblotting of GST the samples were diluted 1:10.

Affinity isolation experiments with recombinant proteins

Proteins were isolated as described above. GST-fusion proteins were eluted from the beads. GST (2 µM), GST-Atg8 or its variants were incubated in BB2 (1 x PBS, pH 7.4, 2 mM $MgCl_2$, 0.2% Triton X-100, 20 mM imidazole [Merck, 1.04716]) and Complete protease inhibitors for 2 h at 4°C with 2 µM His_6-Gyp1 immobilized on Ni-NTA agarose. Samples of the BB containing the respective GST-fusion were taken (Input). After bead sedimentation, the supernatant was removed. Beads were washed 4 times with BB2. Beads were then resuspended in 50 µl Laemmli sample buffer (Bound). Inputs correspond to 4% of the bound fraction. For immunoblotting, 10 µl of samples were used.

Immunoprecipitation of GFP-fusion proteins

Corresponding strains were grown to mid-log phase in appropriate selection medium. For induction of *ATG8*, expressed

from the *GAL1* promoter, galactose (Sigma, G0750)-containing medium was used. Approximately 150–200 OD_{600} units of cells were used for GFP-TRAPs with the different GAPs, the Atg8 variants and Gyp1[AIM] mutants. Approximately 1000 OD_{600} units of cells were used when Atg1-GFP and GFP-Atg8 were expressed from the endogenous promoters. Cells were harvested and glass bead lysed in BB3 (1 x PBS, pH 7.4, 0.2 M sorbitol [Roth, 6213.2], 5 mM $MgCl_2$, 1% Triton X-100 and Complete protease inhibitors). Cells (120–250 OD_{600} units) were analyzed after 24–30 h growth in 2% lactate (Roth, 8460.1) medium without methionine to induce expression of GFP-Atg32 from the *MET25* promoter for the GFP-TRAPs with GFP-Atg32. A different lysis buffer (50 mM Tris-HCl [Roth, 5429.2], pH 7.5, 100 mM NaCl [Roth, 3957.2], 0.1 mM EDTA [Roth, 8043.1], 0.2% Trition X-100, 1 x Phos-STOP [Roche, 4906845001] and Complete protease inhibitors) was applied. For immunoblot analysis, samples of cleared lysate were removed. The rest of the lysate was incubated with equilibrated beads carrying GFP-binding protein (ChromoTek, GFP-Trap_A GTA-20) for 2 h at 4°C under constant mixing. The beads were washed 4 times with BB3. Bound proteins were eluted with 50 µl Laemmli sample buffer (bound). For immunoblotting, 10–15 µl of the samples were loaded and GFP, HA, Flag or Ypt1 antibodies were used. For the GFP-TRAPs with different GAPs, the Atg8 variants and Gyp1[AIM] mutants, the lysate corresponds to 2.5% of the eluate (Bound). For the GFP-TRAPs with Atg8 expressed from the endogenous promoter, the lysate corresponds to 0.083% of the eluate (Bound). For the GFP-TRAP with Atg1-GFP the lysate corresponds to 0.014% of the eluate (Bound). For the GFP-TRAP with GFP-Atg32 the lysate corresponds to 0.84% of the eluate (Bound).

Immunoprecipitation of 2xFlag-Atg8 and Atg19-6xHA

Corresponding strains were grown to log phase in appropriate selection medium. Each strain (250 OD_{600} units of cells) was harvested, washed once with 1 x PBS and glass bead lysed in BB4 (50 mM Tris-HCl, pH 8.0, 150 mM NaCl, 10% glycerol [Roth, 3783.2], 1 x Phos-STOP and Complete protease inhibitors). After lysis, 0.01% Nonidet P40 (Fluka, 74385) was added and lysates were incubated for 20 min at 4°C. Lysates have been cleared and samples of the lysates were taken. The rest of the lysate was incubated with equilibrated HA-agarose (Santa Cruz Biotechnology, sc-7392 AC) for 2 h at 4°C under constant mixing. The beads were washed 5 times with BB4. Bound proteins were eluted with 50 µl Laemmli sample buffer (bound). For immunoblotting, 10 µl of the samples were loaded and Flag and HA antibodies were used. The lysate corresponds to 5.4% of the eluate (Bound).

Fluorescence microscopy

Cells were grown to logarithmic phase (OD_{600}: 1.5–2.5) in corresponding selection medium. For GFP-Atg8, cells were grown to OD_{600} of 4. Cells expressing *MET25p*-mCherry-Gyp1, *MET25p*-GFP-Gyp1 or *MET25p*-mCherry-Atg11 were grown with 0.3 mM methionine (Sigma, M5308) to induce endogenous levels. A DeltaVision Spectris fluorescence microscope (Applied Precision, USA) with a 100 x objective and GFP (excitation wavelengths 475/28 and emission wavelengths 525/50) and mCherry (excitation wavelengths 575/25 and emission wavelengths 632/60) filter set was used. Images were deconvoluted using WoRx software (Applied Precision, USA) and processed with Adobe CS6 or Fiji.

Mitophagy assay

Cells expressing the mitophagy marker mito-GFP (*MET25p*-atp-9/Su9-mtDHFR-GFP; pUG23) were grown in medium containing 2% lactate and lacking methionine for 72 h and samples were taken after 0, 48 and 72 h [87]. Quantification was done after 48 h in lactate medium as detailed below.

Quantification and statistical analysis

Western blots were quantified with a LAS3000 imaging system and the AIDA software. For the GFP-TRAPs and affinity-isolation experiments the ratio of bound fraction and related lysate was calculated and normalized against the amount of indicated bait bound to the beads, except for GFP-Atg32. The wild-type or indicated strain was set to 100%. The amount of Ape1 was determined by calculation of the ratio of Ape1 from the total amount of Ape1 (prApe1 and Ape1). For quantification of the mitophagic rate, the amount of free GFP was divided by the amount of mito-GFP. The ratio of free GFP of the WT cells after 48 h in lactate medium was set to 100%. We used Graph Pad Prism 6 and one sample t-tests to calculate the statistical relevance and included the reference sample in the graph. For fluorescence microscopy, images from at least 3 cultures were taken. For each image, dots/cells were counted. A value of 0.5 dots/cell, for example, indicates that every second cell shows a dot. Number (n) of independent experiments is indicated for each experiment. We used Graph Pad Prism 6 and unpaired two-tailed t-tests to calculate the statistical relevance. Error bars are SEM. The figures are labelled as follows: not significant (ns) or no stars for $P > 0.05$; * for $P < 0.05$; ** for $P < 0.01$; *** for $P < 0.001$; and **** for $P < 0.0001$.

Acknowledgments

We thank Michael Thumm for support and helpful discussions, Henning Urlaub for mass spectrometry and Claudine Kraft for providing the Atg1-GFP plasmid. The Ypt1 antibody, the $Ypt1^{Q67L}$ strains and corresponding WT were a kind gift from Hans Dieter Schmitt.

Author Contributions

A.L. M., P. S. and R.K. performed the experiments shown in the manuscript. R.K. performed the experimental design and wrote the manuscript.

Disclosure statement

No potential conflict of interest was reported by the authors.

Funding

This work was funded by the Deutsche Forschungsgemeinschaft (DFG) under the grant number KR4426/1-1.The authors declare that there is no conflict of interest or financial disclosure.

ORCID

Roswitha Krick http://orcid.org/0000-0002-5483-6108

References

[1] Frake RA, Ricketts T, Menzies FM, et al. Autophagy and neurodegeneration. J Clin Invest. 2015;125:65–74.
[2] Gomes LC, Dikic I. Autophagy in antimicrobial immunity. Mol Cell. 2014;54:224–233.
[3] van der Vaart A, Mari M, Reggiori F. A picky eater: exploring the mechanisms of selective autophagy in human pathologies. Traffic. 2008;9:281–289.
[4] Mizumura K, Choi AMK, Ryter SW. Emerging role of selective autophagy in human diseases. Front Pharmacol. 2014;5:476.
[5] Choi AMK, Ryter SW, Levine B. Autophagy in human health and disease. N Engl J Med. 2013;368:651–662.
[6] Wen X, Klionsky DJ. An overview of macroautophagy in yeast. J Mol Biol. 2016;428:1681–1699.
[7] Farré J-C, Subramani S. Mechanistic insights into selective autophagy pathways: lessons from yeast. Nat Rev Mol Cell Biol. 2016;17:537–552.
[8] Lynch-Day MA, Klionsky DJ. The Cvt pathway as a model for selective autophagy. FEBS Lett. 2010;584:1359–1366.
[9] Kim J, Scott S, Oda M, et al. Transport of a large oligomeric protein by the cytoplasm to vacuole protein targeting pathway. J Cell Biol. 1997;137:609–618.
[10] Kim J, Kamada Y, Stromhaug P, et al. Cvt9/Gsa9 functions in sequestering selective cytosolic cargo destined for the vacuole. J Cell Biol. 2001;153:381–396.
[11] Watanabe Y, Noda NN, Kumeta H, et al. Selective transport of alpha-mannosidase by autophagic pathways: structural basis for cargo recognition by Atg19 and Atg34. J Biol Chem. 2010;285:30026–30033.
[12] Yamasaki A, Noda NN. Structural biology of the Cvt pathway. J Mol Biol. 2017;429:531–542.
[13] Shintani T, Huang W, Stromhaug P, et al. Mechanism of cargo selection in the cytoplasm to vacuole targeting pathway. Dev Cell. 2002;3:825–837.
[14] Yorimitsu T, Klionsky D. Atg11 links cargo to the vesicle-forming machinery in the cytoplasm to vacuole targeting pathway. Mol Biol Cell. 2005;16:1593–1605.
[15] Kamber RA, Shoemaker CJ, Denic V. Receptor-bound targets of selective autophagy use a scaffold protein to activate the Atg1 kinase. Mol Cell. 2015;59:372–381.
[16] Torggler R, Papinski D, Brach T, et al. Two independent pathways within selective autophagy converge to activate Atg1 kinase at the vacuole. Mol Cell. 2016;64:1–39.
[17] He C, Song H, Yorimitsu T, et al. Recruitment of Atg9 to the preautophagosomal structure by Atg11 is essential for selective autophagy in budding yeast. J Cell Biol. 2006;175:925–935.
[18] Lipatova Z, Belogortseva N, Zhang XQ, et al. Regulation of selective autophagy onset by a Ypt/Rab GTPase module. Proc Natl Acad Sci USA. 2012;109:6981–6986.
[19] Kakuta S, Yamamoto H, Negishi L, et al. Atg9 vesicles recruit vesicle-tethering proteins Trs85 and Ypt1 to the autophagosome formation site. J Biol Chem. 2012;287:44261–44269.
[20] Backues SK, Orban DP, Bernard A, et al. Atg23 and Atg27 act at the early stages of Atg9 trafficking in S. cerevisiae. Traffic. 2015;16:172–190.
[21] Wang J, Menon S, Yamasaki A, et al. Ypt1 recruits the Atg1 kinase to the preautophagosomal structure. Proc Natl Acad Sci USA. 2013;110:9800–9805.
[22] Lynch-Day MA, Bhandari D, Menon S, et al. Trs85 directs a Ypt1 GEF, TRAPPIII, to the phagophore to promote autophagy. Proc Natl Acad Sci USA. 2010;107:7811–7816.
[23] Shirahama-Noda K, Kira S, Yoshimori T, et al. TRAPPIII is responsible for vesicular transport from early endosomes to golgi, facilitating Atg9 cycling in autophagy. J Cell Sci. 2013;126:4963–4973.
[24] Jones S, Newman C, Liu F, et al. The TRAPP complex is a nucleotide exchanger for Ypt1 and Ypt31/32. Mol Biol Cell. 2000;11:4403–4411.
[25] Wang W, Sacher M, Ferro-Novick S. TRAPP stimulates guanine nucleotide exchange on Ypt1p. J Cell Biol. 2000;151:289–296.
[26] Meiling-Wesse K, Epple UD, Krick R, et al. Trs85 (Gsg1), a component of the TRAPP complexes, is required for the organization of the preautophagosomal structure during selective autophagy via the Cvt pathway. J Biol Chem. 2005;280:33669–33678.
[27] Nazarko T, Huang J, Nicaud J, et al. Trs85 is required for macroautophagy, pexophagy and cytoplasm to vacuole targeting in Yarrowia lipolytica and Saccharomyces cerevisiae. Autophagy. 2005;1:37–45.
[28] Lipatova Z, Majumdar U, Segev N. Trs33-containing TRAPP IV: a novel autophagy-specific Ypt1 GEF. Genetics. 2016;204:1117–1128.
[29] Thomas LL, Joiner AMN, Fromme JC. The TRAPPIII complex activates the GTPase Ypt1 (Rab1) in the secretory pathway. J Cell Biol. 2018;217:283–298.
[30] Szatmari Z, Sass M. The autophagic roles of Rab small GTPases and their upstream regulators: A review. Autophagy. 2014;10:1154–1166.
[31] Stenmark H. Rab GTPases as coordinators of vesicle traffic. Nat Rev Mol Cell Biol. 2009;10:513–525.
[32] Müller MP, Goody RS. Molecular control of Rab activity by GEFs, GAPs and GDI. Small GTPases. 2017;13:1–17.
[33] Lafourcade C, Galan JM, Gloor Y, et al. The GTPase-activating enzyme Gyp1p is required for recycling of internalized membrane material by inactivation of the Rab/Ypt GTPase Ypt1p. Mol Cell Biol. 2004;24:3815–3826.
[34] Du -L-L, Novick P, Pfeffer SR. Yeast Rab GTPase-activating protein Gyp1p localizes to the golgi apparatus and is a negative regulator of Ypt1p. Mol Biol Cell. 2001;12:1215–1226.
[35] De Antoni A, Schmitzova J, Trepte HH, et al. Significance of GTP hydrolysis in Ypt1p-regulated endoplasmic reticulum to golgi transport revealed by the analysis of two novel Ypt1-GAPs. J Biol Chem. 2002;277:41023–41031.
[36] Kramer MH, Farré J-C, Mitra K, et al. Active interaction mapping reveals the hierarchical organization of autophagy. Mol Cell. 2017;65:761–765.
[37] Suzuki K, Kubota Y, Sekito T, et al. Hierarchy of Atg proteins in pre-autophagosomal structure organization. Genes Cells. 2007;12:209–218.
[38] Araki Y, Ku W-C, Akioka M, et al. Atg38 is required for autophagy-specific phosphatidylinositol 3-kinase complex integrity. J Cell Biol. 2013;203:299–313.
[39] Jao CC, Ragusa MJ, Stanley RE, et al. A HORMA domain in Atg13 mediates PI 3-kinase recruitment in autophagy. Proc Natl Acad Sci USA. 2013;110:5486–5491.
[40] Suzuki SW, Yamamoto H, Oikawa Y, et al. Atg13 HORMA domain recruits Atg9 vesicles during autophagosome formation. Proc Natl Acad Sci USA. 2015;112:3350–3355.
[41] Krick R, Busse RA, Scacioc A, et al. Structural and functional characterization of the two phosphoinositide binding sites of PROPPINs, a β-propeller protein family. Proc Natl Acad Sci USA. 2012;109:E2042–9.
[42] Juris L, Montino M, Rube P, et al. PI3P binding by Atg21 organises Atg8 lipidation. Embo J. 2015;34:955–973.
[43] Noda NN, Kumeta H, Nakatogawa H, et al. Structural basis of target recognition by Atg8/LC3 during selective autophagy. Genes Cells. 2008;13:1211–1218.

[44] Nakatogawa H, Ichimura Y, Ohsumi Y. Atg8, a ubiquitin-like protein required for autophagosome formation, mediates membrane tethering and hemifusion. Cell. 2007;130:165–178.
[45] Xie Z, Nair U, Klionsky DJ. Atg8 controls phagophore expansion during autophagosome formation. Mol Biol Cell. 2008;19:3290–3298.
[46] Weidberg H, Shvets E, Shpilka T, et al. LC3 and GATE-16/GABARAP subfamilies are both essential yet act differently in autophagosome biogenesis. Embo J. 2010;29:1792–1802.
[47] Weidberg H, Shpilka T, Shvets E, et al. LC3 and GATE-16 N termini mediate membrane fusion processes required for autophagosome biogenesis. Dev Cell. 2011;20:444–454.
[48] Nair U, Yen W-L, Mari M, et al. A role for Atg8–PE deconjugation in autophagosome biogenesis. Autophagy. 2012;8:780–793.
[49] Farré J-C, Burkenroad A, Burnett SF, et al. Phosphorylation of mitophagy and pexophagy receptors coordinates their interaction with Atg8 and Atg11. EMBO Rep. 2013;14:441–449.
[50] Kaufmann A, Beier V, Franquelim HG, et al. Molecular mechanism of autophagic membrane-scaffold assembly and disassembly. Cell. 2014;156:469–481.
[51] Noda NN, Ohsumi Y, Inagaki F. Atg8-family interacting motif crucial for selective autophagy. FEBS Lett. 2010;584:1379–1385.
[52] Alemu EA, Lamark T, Torgersen KM, et al. ATG8 family proteins act as scaffolds for assembly of the ULK complex: sequence requirements for LC3-interacting region (LIR) motifs. J Biol Chem. 2012;287:39275–39290.
[53] Nakatogawa H, Ohbayashi S, Sakoh-Nakatogawa M, et al. The autophagy-related protein kinase Atg1 interacts with the ubiquitin-like protein Atg8 via the Atg8 family interacting motif to facilitate autophagosome formation. J Biol Chem. 2012;287:28503–28507.
[54] Shaid S, Brandts CH, Serve H, et al. Ubiquitination and selective autophagy. Cell Death Differ. 2012;20:21–30.
[55] Abreu S, Kriegenburg F, Gomez-Sanchez R, et al. Conserved Atg8 recognition sites mediate Atg4 association with autophagosomal membranes and Atg8 deconjugation. EMBO Rep. 2017;18:765–780.
[56] Krick R, Bremer S, Welter E, et al. Cdc48/p97 and Shp1/p47 regulate autophagosome biogenesis in concert with ubiquitin-like Atg8. J Cell Biol. 2010;190:965–973.
[57] Kalvari I, Tamura N, Oku M, et al. iLIR: A web resource for prediction of Atg8-family interacting proteins. Autophagy. 2014;10:913–925.
[58] Albert S. Identification of the catalytic domains and their functionally critical arginine residues of two yeast GTPase-activating proteins specific for Ypt/Rab transport GTPases. Embo J. 1999;18:5216–5225.
[59] Longatti A, Lamb CA, Razi M, et al. TBC1D14 regulates autophagosome formation via Rab11- and ULK1-positive recycling endosomes. J Cell Biol. 2012;197:659–675.
[60] Lamb CA, Nuhlen S, Judith D, et al. TBC1D14 regulates autophagy via the TRAPP complex and ATG9 traffic. Embo J. 2016;35:281–301.
[61] Baba M, Osumi M, Scott SV, et al. Two distinct pathways for targeting proteins from the cytoplasm to the vacuole/lysosome. J Cell Biol. 1997;139:1687–1695.
[62] Richardson CJ, Jones S, Litt RJ, et al. GTP hydrolysis is not important for Ypt1 GTPase function in vesicular transport. Mol Cell Biol. 1998;18:827–838.
[63] Brett CL, Plemel RL, Lobingier BT, et al. Efficient termination of vacuolar Rab GTPase signaling requires coordinated action by a GAP and a protein kinase. J Cell Biol. 2008;182:1141–1151.
[64] Barth H, Meiling-Wesse K, Epple UD, et al. Mai1p is essential for maturation of proaminopeptidase I but not for autophagy. FEBS Lett. 2002;512:173–179.
[65] Welter E, Thumm M, Krick R. Quantification of nonselective bulk autophagy in S. cerevisiae using Pgk1-GFP. Autophagy. 2010;6:794–797.
[66] Ishihara N, Hamasaki M, Yokota S, et al. Autophagosome requires specific early Sec proteins for its formation and NSF/SNARE for vacuolar fusion. Mol Biol Cell. 2001;12:3690–3702.
[67] Reggiori F, Wang C, Nair U, et al. Early stages of the secretory pathway, but not endosomes, are required for Cvt vesicle and autophagosome assembly in Saccharomyces cerevisiae. Mol Biol Cell. 2004;15:2189–2204.
[68] Kanki T, Wang K, Cao Y, et al. Atg32 is a mitochondrial protein that confers selectivity during mitophagy. Dev Cell. 2009;17:98–109.
[69] Pan X, Eathiraj S, Munson M, et al. TBC-domain GAPs for Rab GTPases accelerate GTP hydrolysis by a dual-finger mechanism. Nature. 2006;442:303–306.
[70] Shintani T, Klionsky D. Cargo proteins facilitate the formation of transport vesicles in the cytoplasm to vacuole targeting pathway. J Biol Chem. 2004;279:29889–29894.
[71] Kihara A, Noda T, Ishihara N, et al. Two distinct Vps34 phosphatidylinositol 3-kinase complexes function in autophagy and carboxypeptidase Y sorting in saccharomyces cerevisiae. J Cell Biol. 2001;152:519–530.
[72] Obara K, Sekito T, Ohsumi Y. Assortment of phosphatidylinositol 3-kinase complexes–atg14p directs association of complex I to the pre-autophagosomal structure in saccharomyces cerevisiae. Mol Biol Cell. 2006;17:1527–1539.
[73] Kern A, Dikic I, Behl C. The integration of autophagy and cellular trafficking pathways via RAB GAPs. Autophagy. 2015;11:2393–2397.
[74] Sacher M, Barrowman J, Wang W, et al. TRAPP I implicated in the specificity of tethering in ER-to-Golgi transport. Mol Cell. 2001;7:433–442.
[75] Zou S, Liu Y, Zhang XQ, et al. Modular TRAPP complexes regulate intracellular protein trafficking through multiple Ypt/Rab GTPases in saccharomyces cerevisiae. Genetics. 2012;191:451–460.
[76] Bacon RA, Salminen A, Ruohola H, et al. The GTP-binding protein Ypt1 is required for transport in vitro: the Golgi apparatus is defective in ypt1 mutants. J Cell Biol. 1989;109:1015–1022.
[77] Stephan JS, Yeh -Y-Y, Ramachandran V, et al. The Tor and PKA signaling pathways independently target the Atg1/Atg13 protein kinase complex to control autophagy. Proc Natl Acad Sci USA. 2009;106:17049–17054.
[78] Kamada Y, Yoshino K-I, Kondo C, et al. Tor directly controls the Atg1 kinase complex to regulate autophagy. Mol Cell Biol. 2010;30:1049–1058.
[79] Noda NN, Fujioka Y. Atg1 family kinases in autophagy initiation. Cell Mol Life Sci. 2015;72:3083–3096.
[80] Kraft C, Kijanska M, Kalie E, et al. Binding of the Atg1/ULK1 kinase to the ubiquitin-like protein Atg8 regulates autophagy. Embo J. 2012;31:3691–3703.
[81] Popovic D, Akutsu M, Novak I, et al. Rab GAPs in Autophagy: regulation of endocytic and autophagy pathways by direct binding to human ATG8 modifiers. Mol Cell Biol. 2012;32:1733–1744.
[82] Sawa-Makarska J, Abert C, Romanov J, et al. Cargo binding to Atg19 unmasks additional Atg8 binding sites to mediate membrane–cargo apposition during selective autophagy. Nat Cell Biol. 2014;16:425–433.
[83] Janke C, Magiera M, Rathfelder N, et al. A versatile toolbox for PCR-based tagging of yeast genes: new fluorescent proteins, more markers and promoter substitution cassettes. Yeast. 2004;21:947–962.
[84] Longtine M, McKenzie A, Demarini D, et al. Additional modules for versatile and economical PCR-based gene deletion and modification in saccharomyces cerevisiae. Yeast. 1998;14:953–961.
[85] Meiling-Wesse K, Barth H, Voss C, et al. Atg21 is required for effective recruitment of Atg8 to the preautophagosomal structure during the Cvt pathway. J Biol Chem. 2004;279:37741–37750.
[86] Barth H, Thumm M. A genomic screen identifies AUT8 as a novel gene essential for autophagy in the yeast saccharomyces cerevisiae. Gene. 2001;274:151–156.
[87] Welter E, Montino M, Reinhold R, et al. Uth1 is a mitochondrial inner membrane protein dispensable for post-log-phase and rapamycin-induced mitophagy. FEBS J. 2013;280:4970–4982.

[88] Sikorski R, Hieter P. A system of shuttle vectors and yeast host strains designed for efficient manipulation of DNA in saccharomyces cerevisiae. Genetics. 1989;122:19–27.
[89] Amar N, Lustig G, Ichimura Y, et al. Two newly identified sites in the ubiquitin-like protein Atg8 are essential for autophagy. EMBO Rep. 2006;7:635–642.
[90] Thumm M, Egner R, Koch B, et al. Isolation of autophagocytosis mutants of saccharomyces cerevisiae. FEBS Lett. 1994;349:275–280.
[91] Straub M, Bredschneider M, Thumm M. AUT3, a serine/threonine kinase gene, is essential for autophagocytosis in saccharomyces cerevisiae. J Bacteriol. 1997;179:3875–3883.